Cationic Anthraquinone Derivatives as Catalytic DNA Photonucleases: Mechanisms for DNA Damage and Quinone Recycling

Bruce Armitage, Changjun Yu, Chelladurai Devadoss, and Gary B. Schuster*,†

Contribution from the Department of Chemistry, Roger Adams Laboratory, University of Illinois, Urbana, Illinois 61801

Received April 15, 1994®

Abstract: Ammonium-substituted anthraquinone derivatives have been found to catalyze DNA cleavage upon irradiation with 350 nm light. Picosecond laser spectroscopy demonstrates that the excited quinones react with DNA by two separate oxidative pathways: electron transfer from a nearby base and hydrogen atom abstraction from the deoxyribose component of the nucleic acid backbone. Photo-oxidation of DNA by either pathway yields the one-electron-reduced form of the quinone as a byproduct. Back electron transfer from the reduced quinone to the oxidized base is the predominant decay path for the reduced quinone formed by the electron transfer pathway while that formed by hydrogen atom abstraction is converted back to the ground-state, fully oxidized form by reduction of molecular oxygen. The resulting superoxide anion is detected by its reduction of cytochrome *c*. Comparison of the spectroscopic data for two quinones with significantly different cleavage efficiencies suggests that DNA cleavage by these quinone reagents results from the hydrogen-abstraction chemistry. The laser experiments further indicate that the quinone completes one cycle of excitation, oxidation of DNA, and reduction of oxygen within 10 μs, illustrating the potential utility of these agents for double-stranded cleavage of DNA.

Introduction

The ability to perform double-stranded (ds) cleavage of DNA is crucial to many molecular biological techniques such as gene isolation and production of recombinant DNA vectors.[1] Currently, naturally occurring restriction enzymes (endonucleases)[2] are utilized for these applications, but because of their relatively short DNA recognition sequences (4–8 base pairs), endonucleases are most suitable for use with DNA in the kilobase pair range (i.e., bacterial and viral DNA). Consequently, there is widespread interest in the development of synthetic nucleases[3] with extended recognition sequences and therefore applicability to genomic DNA in the megabase pair range. Substantial ability has been developed to extend sequence recognition through the use of triplex-forming linear[4] and circular[5] oligonucleotides as well as peptide nucleic acids.[6] Coupling of these recognition elements to efficient ds-cleavage agents should lead to the production of useful synthetic endonucleases.

In order for a single molecule (or supermolecule) to cleave both strands of duplex DNA at a given site, the cleavage moiety must be either bifunctional or recyclable. Natural endonucleases achieve ds cleavage by the first strategy: the enzymes bind to their recognition sequences as dimers with one subunit cleaving one strand and the other subunit cleaving the complementary strand.[7] Binding as dimers accounts for the prevalence of palindromic recognition sequences for these enzymes. Intriguing synthetic nucleases which exhibit significant ds cleavage of supercoiled plasmid DNA have been reported by Dervan[8] and Barton.[9] These molecules are bifunctional, containing two covalently linked transition metal complexes which initiate cleavage by oxidation of the DNA backbone. More recently, synthetic analogs of the enediyne antibiotics have been reported to initiate ds cleavage.[10] Upon reductive activation, these molecules are converted into diradicals which can attack both strands of duplex DNA at a given site. With regard to structural and synthetic simplicity, cleavage by a recyclable nuclease is an appealing alternative to these more elaborate bifunctional systems.

We are currently exploring a variety of cationic anthraquinone (AQ) derivatives as recyclable DNA photonucleases (i.e., compounds which initiate DNA strand cleavage upon irradiation). The logic for utilizing AQ is 3-fold: (*i*) The planar, aromatic skeleton of AQ should promote binding to DNA by intercalation between adjacent base pairs as observed for both naturally occurring[11] (e.g., the anthracycline antibiotics) and other synthetic[12] AQ derivatives. (*ii*) Excited-state AQ derivatives are known to be good oxidants.[13] Cleavage of DNA can be initiated

† Present address: School of Chemistry and Biochemistry, Georgia Institute of Technology, Atlanta, GA 30332-0400.

® Abstract published in *Advance ACS Abstracts*, October 1, 1994.

(1) (a) Maniatis, T.; Fritsch, E. F.; Sambrook, J. *Molecular Cloning. A Laboratory Manual*; Cold Spring Harbor Laboratory: Cold Spring Harbor, NY, 1982. (b) Watson, J. D.; Tooze, J.; Kurtz, D. T. *Recombinant DNA: A Short Course*; W. H. Freeman and Co.: New York, 1983.

(2) (a) Smith, H. O. *Science* **1979**, *205*, 455–462. (b) Modrich, P. *Crit. Rev. Biochem.* **1982**, *13*, 288–323. (c) Roberts, R. J. *Nucleic Acids Res.* **1983**, *11*, R135–R167.

(3) For selected examples of synthetic nucleases, see: (a) Sigman, D. S.; Mazumder, A.; Perrin, D. M. *Chem. Rev.* **1993**, *93*, 2295–2316. (b) Sitlani, A.; Long, E. C.; Pyle, A. M.; Barton, J. K. *J. Am. Chem. Soc.* **1992**, *114*, 2303–2312. (c) Hertzberg, R. P.; Dervan, P. B. *Biochemistry* **1984**, *23*, 3934–3945. (d) Nielsen, P. E.; Jeppesen, C.; Egholm, M.; Buchardt, O. *Biochemistry* **1988**, *27*, 6338–6343. (e) Nagai, K.; Carter, B. J.; Xu, J.; Hecht, S. M. *J. Am. Chem. Soc.* **1991**, *113*, 5099–5100. (f) Nicolau, K. C.; Maligres, P.; Shin, J.; de Leon, E.; Rideout, D. *J. Am. Chem. Soc.* **1990**, *112*, 7825–7826. (g) Neyhart, G. A.; Grover, N.; Smith, S. R.; Kalsbeck, W. A.; Fairley, T. A.; Cory, M.; Thorp, H. H. *J. Am. Chem. Soc.* **1993**, *115*, 4423–4428.

(4) (a) Moser, H. E.; Dervan, P. B. *Science* **1987**, *238*, 645–650. (b) Beal, P. A.; Dervan, P. B. *J. Am. Chem. Soc.* **1992**, *114*, 4976–4982. (c) Thuong, N. T.; Hélène, C. *Angew. Chem., Int. Ed. Engl.* **1993**, *32*, 666–690.

(5) Prakash, G.; Kool, E. T. *J. Am. Chem. Soc.* **1992**, *114*, 3523–3527.

(6) Nielsen, P. E.; Egholm, M.; Berg, R. H.; Buchardt, O. *Science* **1991**, *254*, 1497–1500.

(7) (a) Rosenberg, J. *Curr. Opin. Struct. Biol.* **1991**, *1*, 104–113. (b) Heitman, J. *BioEssays* **1992**, *14*, 445–454.

(8) Schultz, P. G.; Dervan, P. B. *J. Am. Chem. Soc.* **1983**, *105*, 7748–7750.

(9) Basile, L. A.; Barton, J. K. *J. Am. Chem. Soc.* **1987**, *109*, 7548–7550.

(10) For a review, see: Nicolau, K. C.; Smith, A. L.; Yue, E. W. *Proc. Natl. Acad. Sci. U.S.A.* **1993**, *90*, 5881–5888.

(11) (a) Quigley, G. J.; Wang, A. H.-J.; Ughetto, G.; van der Marel, G.; van Boom, J. H.; Rich, A. *Proc. Natl. Acad. Sci. U.S.A.* **1980**, *77*, 7204–7208. (b) Neidle, S. *Prog. Med. Chem.* **1979**, *16*, 151–220. (c) Brown, J. R. *Prog. Med. Chem.* **1978**, *15*, 125–164. (d) Sun, D.; Hansen, M.; Clement, J. J.; Hurley, L. H. *Biochemistry* **1993**, *32*, 8068–8074.

0002-7863/94/1516-9847$04.50/0

Chart 1

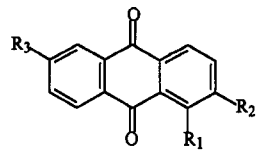

α-substituted AQs

AQC(1) : $R_1 = CONH(CH_2)_4NH_3^+$, $R_2 = R_3 = H$

AQS(1) : $R_1 = SO_2NH(CH_2)_4NH_3^+$, $R_2 = R_3 = H$

β-substituted AQs

AQC(2) : $R_2 = CONH(CH_2)_4NH_3^+$, $R_1 = R_3 = H$

AQS(2) : $R_2 = SO_2NH(CH_2)_4NH_3^+$, $R_1 = R_3 = H$

AQDS(2,6) : $R_2 = R_3 = SO_2NH(CH_2)_4NH_3^+$, $R_1 = H$

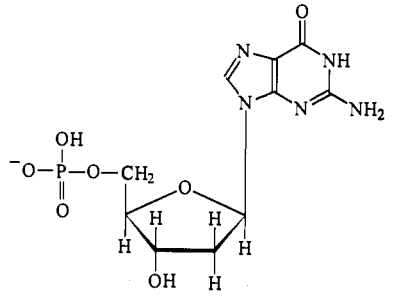

dGMP

by oxidation of the poly(sugar–phosphate) backbone,[14] a process which intercalated AQ could trigger by photoinduced hydrogen atom abstraction from a nearby deoxyribose unit or by electron transfer from a base. (*iii*) Quinones are very stable to repeated cycling through oxidized and reduced forms. Indeed, this feature is exploited in natural systems which employ quinones to shuttle electrons and protons across biomembranes during photosynthesis and respiration.[15] Thus the reduced quinone which would be expected to result from photo-oxidation of the DNA backbone should be readily oxidized back to its initial form without significant decomposition.

Our research group recently reported photocleavage of supercoiled plasmid DNA by the carboxamide-linked ammonium anthraquinone derivative AQC(2)[16] (see Chart 1). Irradiation of this compound gave predominantly single-stranded (ss) cleavage of the DNA, but a low level of double-stranded (ds) cleavage was also detected, suggestive of recycling of the quinone nuclease. Herein, we describe a series of anthraquinone derivatives which function as catalytic DNA photonucleases. While numerous other examples of photonucleases already exist,[17] none exhibits the ability to turn over and thus perform ds cleavage. Furthermore, few mechanistic studies have been reported for the earlier systems.

We present results from investigations into the mechanistic details of the AQ photonuclease cleavage chemistry. Laser spectroscopic experiments ranging from the picosecond to microsecond time scales allow us to follow the quinone through one cycle of DNA damage. The quinone appears to photo-oxidize DNA by two distinct pathways: (*i*) hydrogen atom abstraction from deoxyribose and (*ii*) electron abstraction from individual DNA bases. In principle, either of these pathways could lead to cleavage of the DNA backbone. While the vast majority of known chemical nucleases initiate cleavage via the former route, studies involving radiolysis of single-stranded and double-stranded DNA have demonstrated significant cleavage of the nucleic acid backbone under conditions where oxidized bases are formed.[18] Regarding the AQ photonucleases, laser spectroscopic data obtained for the carboxamide AQC(2) and the disulfonamide AQDS(2,6) are more consistent with a cleavage mechanism in which H abstraction from deoxyribose is the key step, while the electron transfer pathway is predominantly an energy-wasting cycle. Moreover, the cleavage efficiency varies considerably within the series of photonucleases and appears to depend strongly on the orientation of the bound quinone, as would be expected for an H-abstraction process. Further experiments have led to elaboration of the mechanism to include recycling of the quinones, a process which is critical to their function as catalytic nucleases.

Results

The syntheses of the water-soluble cationic AQ derivatives shown in Chart 1 proceed readily from the carbonyl or sulfonyl chlorides and the appropriate mono-boc-protected diamine. The nomenclature used for these compounds is indicated in the chart. Additionally, substitution at carbons 1 and 2 of the AQ skeleton will be referred to as α- and β-substitution, respectively, for clarity and consistency with literature usage.[19]

(I) Characterization of the DNA/Quinone Complexes. (A) Equilibrium Binding Constants. Binding of the anthraquinone reagents to calf thymus (CT) DNA was investigated by UV–vis and fluorescence spectroscopies. The lowest energy absorption band for the β-substituted quinones exhibits a pronounced hypochromic effect (20–30%) as well as a modest bathochromic shift (3–4 nm) in the presence of DNA (A representative example is shown in Figure 1; data for other quinones are collected in Table 1). Equilibrium binding constants for AQC(2), AQS(2), and AQDS(2,6) were measured by titrating a buffered solution (10 mM phosphate, 100 mM NaCl, pH = 7.2) of each quinone with DNA and monitoring the decrease in absorbance of the sample. Scatchard analysis[20] of the data yields a linear fit in each case, indicative of binding to DNA by a single mode. The resulting binding constants range from 6.9×10^4 to 9.3×10^4 M^{-1} (Table 2). The similarity among these values indicates that binding of the quinone to DNA is relatively insensitive to the nature of the amide linker (carboxamide or sulfonamide) and to the number of cationic tails (one or two), thereby suggesting that direct interaction between the DNA and the AQ skeleton is the

(12) (a) Islam, S. A.; Neidle, S.; Gandecha, B. M.; Partridge, M.; Patterson, L. H.; Brown, J. R. *J. Med. Chem.* **1985**, *28*, 857–864. (b) Islam, S. A.; Neidle, S.; Gandecha, B. M.; Brown, J. R. *Biochem. Pharmacol.* **1983**, *32*, 2801–2808. (c) Palumbo, M.; Magno, S. M. *Stud. Biophys.* **1984**, *104*, 123–130. (d) Takenaka, S.; Ihara, T.; Hamano, M.; Takagi, M. *J. Chem. Soc., Chem. Commun.* **1990**, 1271–1273. (e) Agbandje, M.; Jenkins, T. C.; McKenha, R.; Reszka, A. P.; Neidle, S. *J. Med. Chem.* **1992**, *35*, 1418–1429. (f) Tanious, F. A.; Jenkins, T. C.; Neidle, S.; Wilson, W. D. *Biochemistry* **1992**, *31*, 11632–11640.

(13) Levin, P. P.; Kuz'min, V. A. *Russ. Chem. Rev.* **1987**, *56*, 307–325.

(14) Stubbe, J.; Kozarich, J. W. *Chem. Rev.* **1987**, *87*, 1107–1136.

(15) *Function of Quinones in Energy Conserving Systems*; Trumpower, B. L., Ed.; Academic Press: New York, 1982.

(16) Koch, T.; Ropp, J. D.; Sligar, S. G.; Schuster, G. B. *Photochem. Photobiol.* **1993**, *58*, 554–558.

(17) Photonucleases: (a) Sitlani, A.; Long, E. C.; Pyle, A. M.; Barton, J. K. *J. Am. Chem. Soc.* **1992**, *114*, 2303–2312. (b) Krotz, A. H.; Hudson, B. P.; Barton, J. K. *J. Am. Chem. Soc.* **1993**, *115*, 12577–12578. (c) Sitlani, A.; Dupureur, C. M.; Barton, J. K. *J. Am. Chem. Soc.* **1993**, *115*, 12589–12590. (d) Nielsen, P. E.; Jeppesen, C.; Egholm, M.; Buchardt, O. *Biochemistry* **1988**, *27*, 6338–6343. (e) Nielsen, P. E.; Hiort, C.; Sönnichsen, S. H.; Buchardt, O.; Dahl, O.; Nordén, B. *J. Am. Chem. Soc.* **1992**, *114*, 4967–4975. (f) Matsugo, S.; Kawanishi, S.; Yamamoto, K.; Sugiyama, H.; Matsuura, T.; Saito, I. *Angew. Chem., Int. Ed. Engl.* **1991**, *30*, 1351–1353. (g) Saito, I.; Takayama, M.; Matsuura, T.; Matsugo, S.; Kawanishi, S. *J. Am. Chem. Soc.* **1990**, *112*, 883–884. (h) Takenaka, S.; Ihara, T.; Takagi, M. *Chem. Lett.* **1992**, 1–4. (i) Quada, J. C., Jr.; Levy, M. J.; Hecht, S. M. *J. Am. Chem. Soc.* **1993**, *115*, 12171–12172. (j) Nishiwaka, E.; Lee, H.; Matsumoto, T.; Toyooka, K.; Sakurai, H.; Shibuya, M. *Tetrahedron Lett.* **1990**, *31*, 1299–1302. (k) Balcker, A. J.; Jazwinski, J.; Lehn, J.-M.; Wilhelm, F. X. *J. Chem. Soc., Chem. Commun.* **1986**, 1035–1037.

(18) (a) Boon, P. J.; Cullis, P. M.; Symons, M. C. R.; Wren, B. W. *J. Chem. Soc., Perkin Trans. 2* **1984**, 1393–1399. (b) von Sonntag, C. In *Physical and Chemical Mechanisms in Molecular Radiation Biology*; Glass, W. A., Varma, M. N., Eds.; Plenum Press: New York, 1991.

(19) *The Chemistry of Quinonoid Compounds*; Patai, S., Ed.; Wiley: London, 1974.

(20) (a) Scatchard, G. *Ann. N. Y. Acad. Sci.* **1949**, *51*, 660–672. (b) Peacocke, A. R.; Skerrett, J. N. H. *Faraday Soc. Trans.* **1956**, *52*, 261–279.

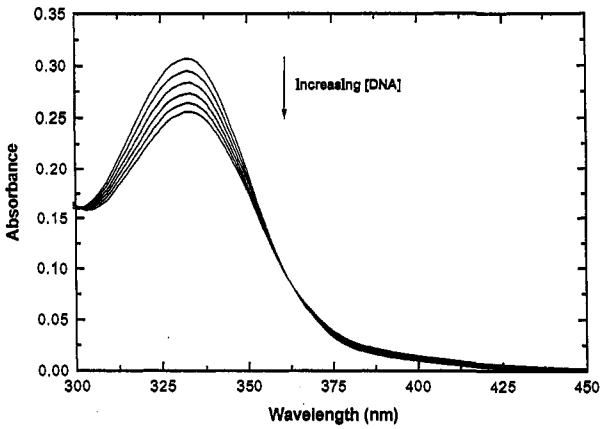

Figure 1. UV–vis titration of AQC(2) with DNA. [AQC(2)] = 40 μM; DNA added in 20 μM (base pair) aliquots.

Table 1. Extinction Coefficients and Percent Hypochromicity for β-Substituted Anthraquinones Dissolved in Phosphate-Buffered Saline (PBS) and Bound to DNA

quinone	$\epsilon_{PBS} \times 10^{-3}$ (M^{-1} cm^{-1})	$\epsilon_{DNA} \times 10^{-3}$ (M^{-1} cm^{-1})	% hyp
AQC(2)	5.5	3.9	30
AQS(2)	5.4	4.2	22
AQDS(2,6)	5.9	4.4	25

Table 2. Equilibrium Constants ($K_{assoc} \times 10^{-4}$ (M^{-1})) for Binding of β-Substituted Anthraquinones to Various DNAs

intercalator	CT DNA[a]	CT DNA[b]	poly-(dG-dC)[b]	poly-(dA-dT)[b]	K_{AT}/K_{GC}
AQC(2)	7.7 ± 1.2	6.2 ± 0.4	8.3 ± 0.9	23.8 ± 1.2	2.9
AQS(2)	6.9 ± 1.3	3.4 ± 0.3	5.9 ± 0.5	22.3 ± 1.1	3.8
AQDS(2,6)	9.3 ± 1.2	13.8 ± 0.2	17.4 ± 0.2	66.8 ± 2.0	3.9
EB	nd[c]	20.4 ± 0.3	34.8 ± 0.5	31.7 ± 0.1	0.9

[a] Determined by UV–vis titration with Scatchard analysis. [b] Determined by fluorescence titration with McGhee–von Hippel analysis. [c] Not determined.

main force for association. On the basis of the significant hypochromicity observed upon binding and by analogy to other AQ derivatives,[11,12] we conclude that these β-substituted AQs bind to DNA by intercalation.

DNA binding by the quinones was also investigated by fluorescence spectroscopy by utilizing an assay in which a given quinone competes with the known intercalator ethidium bromide (EB) for available binding sites.[21] The binding constants obtained by this method agree reasonably well with those resulting from the direct UV–vis titration (Table 2). This technique was also used to measure the association constants for the β-substituted quinones with the synthetic, double-stranded polynucleotides $[poly(dG\text{-}dC)]_2$ and $[poly(dA\text{-}dT)]_2$, in which the purine and pyrimidine bases alternate on both strands. Ethidium exhibits little preference for either DNA (Table 2). However, each of the quinones binds significantly stronger to $[poly(dA\text{-}dT)]_2$, with the sulfonamides displaying a larger preference than the carboxamide (Table 2).

The α-substituted anthraquinones AQC(1) and AQS(1) exhibit significantly weaker binding to DNA than their β-substituted analogs. The hypochromicity observed upon binding to DNA is only 10–15%, a change too small to permit determination of the binding constant by the UV–vis titration method. We attempted to measure the binding constant for AQS(1) by competition with EB. A Scatchard plot for this yielded an approximate binding constant of 1.2×10^4 M^{-1}, indicating that this α-substituted derivative binds at least 5–10 times weaker than the β-substituted anthraquinones.[22]

(21) LePecq, J.-B.; Paoletti, C. *J. Mol. Biol.* **1967**, *27*, 87–106.

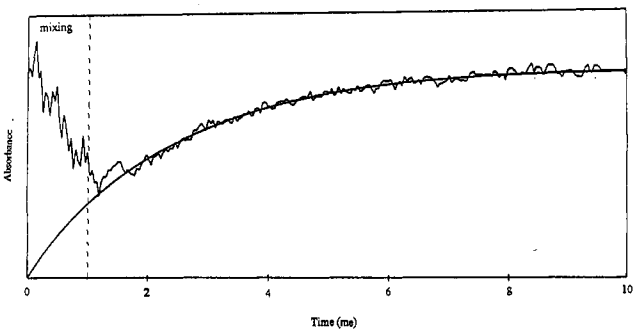

Figure 2. Increase in AQDS(2,6) absorbance upon dissociation from DNA obtained from stopped-flow spectroscopic analysis as described in the Experimental Section. The solid line through the data corresponds to the best fit for a single exponential growth. [AQDS(2,6)] = 0.1 mM, [DNA] = 1.0 mM base pairs.

(B) Kinetic Stability of the Intercalation Complexes. In addition to studying the thermodynamic stability of these systems, we investigated the kinetic stability of the DNA/quinone intercalation complexes by a stopped-flow absorption spectroscopic method.[23] This procedure involves rapid mixing of a solution containing DNA-bound quinone with a second solution that contains concentrated, micellar sodium dodecyl sulfate (SDS). As the cationic quinone dissociates from the DNA (the rate-limiting step[24]), it is irreversibly trapped by the anionic SDS micelles, preventing its reassociation with the DNA. This process produces a time-dependent increase in the absorbance of the quinone since release from the DNA relieves the hypochromic effect caused by intercalation. The stopped-flow kinetic data for AQDS(2,6) can be satisfactorily fit by a single exponential function, again indicative of a single binding mode for this quinone (Figure 2).[25] The resulting dissociation constant (k_d) is 360 s^{-1}. For the monosubstituted derivatives AQS(2) and AQC(2), the dissociation rate overlaps with the mixing time of the instrument (ca. 1 ms), preventing precise determination of k_d for these analogs. However, a reliable lower limit of ca. 1000 s^{-1} can be assigned to this rate constant, indicating that dissociation of the disubstituted quinone is retarded by at least a factor of 3. This effect is larger in magnitude than the difference in the thermodynamic stabilities of the DNA–quinone complexes as indicated by their respective association constants. The slower dissociation of AQDS(2,6) is postulated to result from "threading" of this molecule through the intercalation site, placing one cationic tail in the major groove and one in the minor groove with the quinone ring lying approximately parallel to the adjacent base pairs. Association in this manner provides a kinetic barrier to dissociation as the threaded tail serves to hinder release of the molecule from the intercalation site. Qualitatively similar results have been reported for a series of α-substituted amino- and amidoanthraquinone derivatives.[24,12f] Dissociation (k_d) and association ($k_{assoc} = K_{assoc}k_d$) rate constants as well as residence times ($\tau_r = 1/k_d$) are collected in Table 3.

(C) Geometry of the Intercalation Complexes. Information about the geometry of the DNA/quinone intercalation complexes can be obtained from circular dichroism (CD) spectroscopy. Binding of an achiral molecule within a chiral environment, such as that afforded by right-handed double-helical DNA, can lead

(22) However, there also appears to be some chemical quenching of the excited ethidium by AQS(1) under conditions where both should be bound to the DNA. Thus, the association constant given is, at best, an upper limit.

(23) Muller, W.; Crothers, D. M. *J. Mol. Biol.* **1968**, *35*, 251–290.

(24) (a) Wilson, D. W.; Grier, D.; Reimer, R.; Bauman, J. D.; Preston, J. F.; Gabbay, E. J. *J. Med. Chem.* **1976**, *19*, 381–384. (b) Gabbay, E. J.; Grier, D.; Fingerle, R. E.; Reimer, R.; Levy, R.; Pearce, S. W.; Wilson, W. D. *Biochemistry* **1976**, *15*, 2062–2070. (c) Grant, M.; Phillips, D. R. *Mol. Pharmacol.* **1979**, *16*, 357–360. (d) Gandecha, B. M.; Brown, J. R.; Crampton, M. R. *Biochem. Pharmacol.* **1985**, *34*, 733–736.

(25) In principle, dissociation from each of the 10 possible intercalation sites would be characterized by a different rate constant. However, this is beyond the resolution of our instrument.

Table 3. Dissociation Rate Constants (k_d), Association Rate Constants (k_{assoc}), and Residence Times (τ_r) for DNA-Bound Anthraquinones

quinone	k_d (s^{-1})	$k_{assoc} \times 10^{-7}$ (M^{-1} s^{-1})	τ_r (ms)
AQC(2)	>1000	>7.7	<1
AQS(2)	>1000	>6.9	<1
AQDS(2,6)	360 ± 60	3.3	2.8

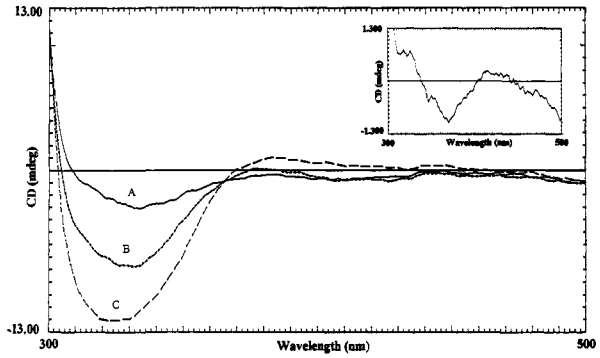

Figure 3. Induced circular dichroism (CD) spectra for (A) AQC(2), (B) AQS(2), and (C) AQDS(2,6) in the presence of 1.6 mM (base pairs) DNA. [Quinone] = 0.2 mM in each case. In the absence of DNA, no CD signal was observed in this region for any of these quinones. Inset: induced CD spectrum for 0.2 mM AQS(1) in the presence of 0.8 mM DNA. Note that the Y-scale is expanded by a factor of 10 in comparison with the main figure.

to induced optical activity for the bound species (ligand).[26] This is manifested in the appearance of a CD absorption band, assignable to the ligand but observed only in the presence of DNA. Provided the ligand absorbs light in a region where the DNA is transparent, it is straightforward to assign the new band to the ligand. This is a well-known effect observed for a variety of DNA intercalators,[26,27] including several AQ derivatives.[12c]

In the absence of DNA, of course, there are no observable CD bands for any of the AQ derivatives we examined. However, each of the β-substituted quinones exhibits an induced CD band upon binding to DNA (Figure 3). There is a significant variation in the intensities of the induced CD bands, with AQDS(2,6) > AQS(2) > AQC(2). Importantly, this order does not parallel that of the respective equilibrium binding constants so the trend in the CD spectra cannot be assigned to differences in the DNA-binding affinities of the AQ derivatives. Furthermore, the extinction coefficients of the quinones when bound to DNA are similar so that differential light absorption cannot be the cause of the variation in their CD spectra. Instead, the intensity variation most likely reflects different geometries for the quinone/DNA intercalation complexes. The nature of these geometrical variations will be discussed in greater detail below.

The α-substituted AQS(1) exhibits a much weaker induced CD spectrum as well as a Cotton band, i.e. splitting into positive and negative absorption bands (Figure 3, inset). Similar results were reported for methylene blue and attributed to multiple binding modes for the dye.[28] (Binding of two dye molecules in close proximity, one by intercalation and one by exterior association, could result in the exciton coupling which gives rise to split CD bands as observed in the inset to Figure 3.) AQS(1) appears to have a similarly complex association behavior with DNA.

(II) DNA Cleavage. (A) Comparison of Cleavage Efficiencies for AQ Reagents. Photocleavage of DNA by AQC(2) was previously demonstrated by conversion of supercoiled plasmid DNA to the circular and linear forms,[16] which are distinguishable

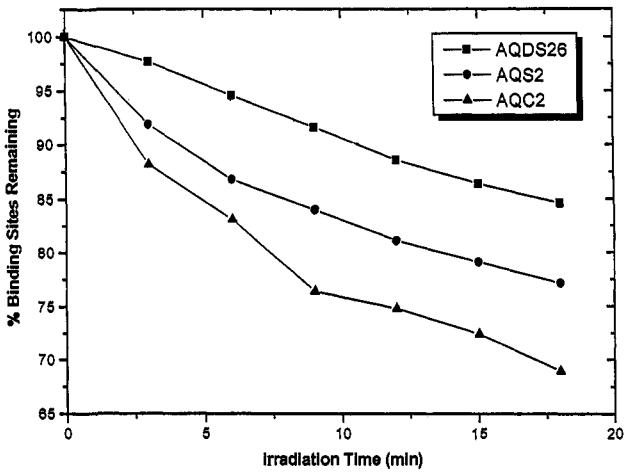

Figure 4. Photocleavage of DNA by AQC(2), AQS(2), and AQDS(2,6). [Quinone] = 19 μM, [DNA] = 250 μM base pairs.

by gel electrophoresis.[29] DNA cleavage by the other quinones shown in Chart 1 has been established by two assays. Qualitatively, cleavage is readily detected by the ability to render CT DNA ethanol soluble upon photolysis in the presence of any of the β-substituted quinones. (Prior to photolysis, addition of 1 aliquot of DNA solution to ethanol causes immediate precipitation of the DNA.) In contrast, neither of the α-substituted quinones degrades DNA to an ethanol-soluble form, even after extensive irradiation. For a quantitative comparison of the cleavage efficiencies of the various quinones, we applied a simple assay for cleavage[30] based on the ca. 20-fold enhancement of the fluorescence intensity exhibited by EB upon intercalation into DNA.[21] The key to the assay is to employ an EB concentration which saturates the DNA. Under conditions where there is excess EB relative to DNA base pairs (e.g., two EBs per DNA base pair, as utilized in this assay), the fluorescence intensity of EB is linearly proportional to the concentration of DNA base pairs. Any process which destroys potential EB binding sites results in a decrease in its fluorescence intensity. Cleavage of the DNA backbone is one such process; this effect forms the basis for an assay of photocleavage by the quinone nucleases. The number of binding sites remaining after irradiation of the quinone is calculated from the initial (no irradiation) and final (EB in solution) fluorescence intensities, as is described in the Experimental Section. Although this method does not directly assay DNA cleavage, it is adequate for comparing the activities of different nucleases.

The cleavage efficiencies for the anthraquinone reagents were investigated under identical conditions using the EB assay. As illustrated in Figure 4, quinones which possess similar binding affinities for CT DNA can exhibit significantly different cleavage efficiencies: AQC(2) cleaves DNA most efficiently with AQS-(2) and AQDS(2,6) being 69% and 20% as fast, respectively.

(B) Catalytic Cleavage of DNA by AQ Photonucleases. Figure 5 illustrates the results of the EB assay for photocleavage of DNA by AQC(2) performed with a ratio of one quinone for every 10 DNA base pairs. If each quinone were to react only once, a maximum of 10% of the available binding sites could be destroyed. (This amount is indicated in Figure 5 by the dashed line at 90% binding sites remaining.) In the experiment, greater than 80% of the binding sites are destroyed during 50 min of irradiation: this observation conclusively demonstrates recycling of the quinone photonuclease. Interestingly, cleavage to this extent requires that most of the DNA exist as either very short duplexes or single-stranded oligomers, consistent with the observation that the products are completely soluble in ethanol. Proof that the

(26) Nordén, B.; Tjerneld, F. *Biopolymers* **1982**, *21*, 1713–1734.
(27) (a) Fredericq, E.; Houssier, C. *Biopolymers* **1972**, *11*, 2281–2308. (b) Li, H. J.; Crothers, D. M. *Biopolymers* **1969**, *8*, 217–235. (c) Fornasiero, D.; Kurucsev, T. *J. Phys. Chem.* **1981**, *85*, 613–618.
(28) Lyng, R.; Härd, T.; Nordén, B. *Biopolymers* **1987**, *26*, 1327–1345.
(29) Thorne, H. V. *J. Mol. Biol.* **1966**, *24*, 203–211.
(30) Cleavage of DNA by the hydroxyl radical has been assayed similarly: (a) Prütz, W. A. *Radiat. Environ. Biophys.* **1984**, *23*, 1–6. (b) Prütz, W. A. *Radiat. Environ. Biophys.* **1984**, *23*, 7–18. (c) Birnboim, H. C.; Jovcak, J. J. *Cancer Res.* **1981**, *41*, 1889–1892.

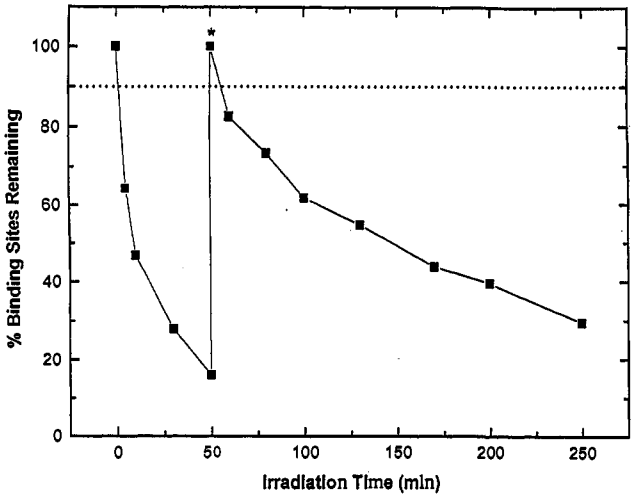

Figure 5. DNA photocleavage by AQC(2) detected by reduced binding of ethidium bromide to the damaged DNA. [AQC(2)] = 26 μM, [DNA] = 260 μM base pairs; cleavage initiated by irradiation in a Rayonet photoreactor (nine lamps, λ = 350 nm). The horizontal dashed line at 90% binding sites remaining corresponds to the theoretical limit for cleavage if the quinone is not recycled. Cleavage beyond this limit is indicative of turnover by the quinone. After 50 min of irradiation, fresh DNA was added (*) and irradiation resumed. The fluorescence recorded at this point was reset to 100%, and subsequent data were normalized accordingly.

quinone has not been inactivated during this reaction comes from addition of a fresh portion of double-stranded DNA to the reaction mixture (the position marked with * in Figure 5). Resumed irradiation without further addition of AQC(2) leads to cleavage of the added DNA.

(C) Photostability of the AQ Photonucleases. When bound to DNA, AQC(2) exhibits excellent photostability. Irradiation to an extent where greater than 30% of potential ethidium bromide binding sites are lost leads to virtually no net consumption of the quinone, as judged by preservation of the quinone absorption at 333 nm (data not shown). In the absence of DNA, irradiation leads to the appearance of a persistent yellow color in the solution and 7% of the quinone absorbance at 333 nm is lost. Thus, binding and reaction of AQC(2) with DNA actually improves the photostability of the quinone.

(III) Investigation of the Cleavage Mechanism. (A) Laser Spectroscopy. Time-resolved laser spectroscopy was utilized in an effort to elucidate the mechanism for DNA cleavage by the AQ photonucleases as well as to gain some insight into why the various quinones exhibit significantly different cleavage efficiencies. Excitation of DNA-intercalated AQC(2) with a 20 ps laser pulse at 355 nm produces a transient species absorbing at λ_{max} = 555 nm within the pulse (Figure 6A). This species decays by approximately 35% and exhibits a progressive blue shift over a period of 200 ps, leaving a residual absorbance at λ_{max} = 545 nm. Then over the next 9.8 ns, there is a slower evolution of the spectrum, with a further blue shift of the maximum to 535 nm and a slight decay on the longer wavelength side of the maximum.

Similar excitation of DNA-intercalated AQDS(2,6) produces a transient species absorbing at λ_{max} = 600 nm within the laser pulse (Figure 6B). Again, this species decays by ca. 40% within 200 ps with a blue shift of the maximum to 585 nm. Over the next 9.8 ns, however, the maximum remains at 585 nm but the absorbance decays by an additional 15%.

The location and shape of the absorption bands shown in Figure 6 are inconsistent with typical triplet–triplet absorption spectra for anthraquinone derivatives, which characteristically exhibit maxima below 400 nm with only tailing absorption in the visible.[31]

(31) (a) Hulme, B. E.; Land, E. J.; Phillips, G. O. *J. Chem. Soc., Faraday Trans. 1* **1972**, *68*, 2003–2012. (b) Harriman, A.; Mills, A. *Photochem. Photobiol.* **1981**, *33*, 619–625.

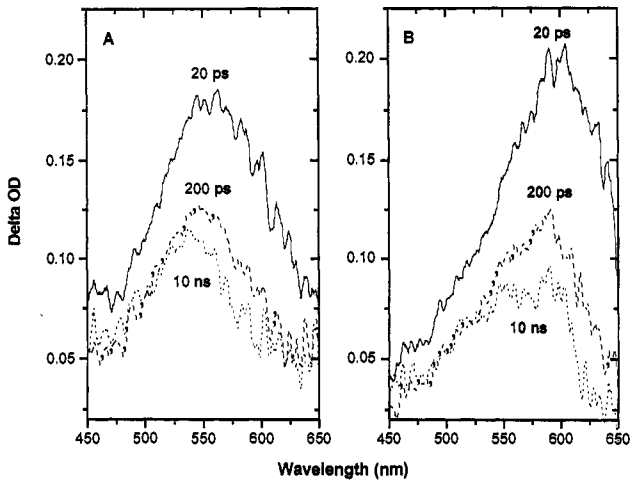

Figure 6. Transient absorbance spectra of calf thymus DNA-intercalated with (A) AQC(2) and (B) AQDS(2,6) recorded at 20 ps, 200 ps, and 10 ns delays after a 355 nm Nd-YAG laser pulse. [Quinone] = 1.5 mM, [DNA] = 7.5 mM in PBS buffer.

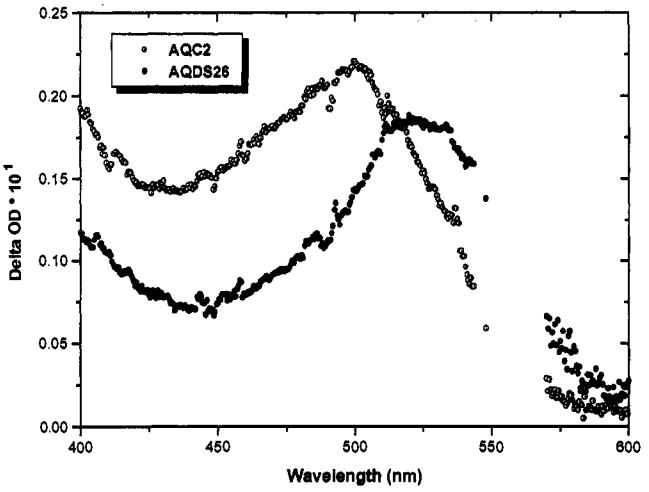

Figure 7. Transient absorbance spectra for AQC(2) and AQDS(2,6) in aqueous sodium nitrite. Spectra were recorded 100 ns after a 308 nm laser pulse. [Quinone] = 0.3 mM, [$NaNO_2$] = 100 mM.

Rather, these bands are similar to that of the one-electron-reduced form of anthraquinone, which absorbs at λ_{max} = 540 nm in acetonitrile.[32] Independent generation of the one-electron-reduced forms of AQC(2) and AQDS(2,6) in water was accomplished by excitation with a 10 ns laser pulse at 308 nm in the presence of 100 mM sodium nitrite. Both quinones exhibit transient absorption bands in the visible, with λ_{max} = 500 and 525 nm for AQC(2) and AQDS(2,6), respectively (Figure 7). We assign these bands to the radical anion form of the quinones, produced by photoinduced electron transfer from the nitrite anion, as observed for a variety of water-soluble anthraquinone derivatives.[33] Excitation of either quinone in the absence of nitrite yields a weak, tailing absorption band in the visible which is most likely due either to the triplet of the quinone or to a hydrated photoproduct (data not shown). The 25 nm difference in λ_{max} for the two radical anions in water is consistent with the differences observed in DNA; the larger disparity observed when the radical anions are bound to the nucleic acid most likely reflects different orientations and sequence preferences for the two quinones: the anthraquinone radical anion is known to be highly solvatochromic, with λ_{max} =

(32) (a) Hamanoue, K.; Yokohama, K.; Kajiwara, Y.; Kimoto, M.; Nakayama, T.; Teranishi, H. *Chem. Phys. Lett.* **1985**, *113*, 207–212. (b) Hamanoue, K.; Nakayama, T.; Sugiura, K.; Teranishi, H.; Washio, M.; Tagawa, S.; Tabata, Y. *Chem. Phys. Lett.* **1985**, *118*, 503–506.

(33) Loeff, I.; Rabani, J.; Treinin, A.; Linschitz, H. *J. Am. Chem. Soc.* **1993**, *115*, 8933–8942. (b) Moore, J. N.; Phillips, D.; Nakashima, N.; Yoshihara, K. *J. Chem. Soc., Faraday Trans. 2* **1987**, *83*, 1487–1508.

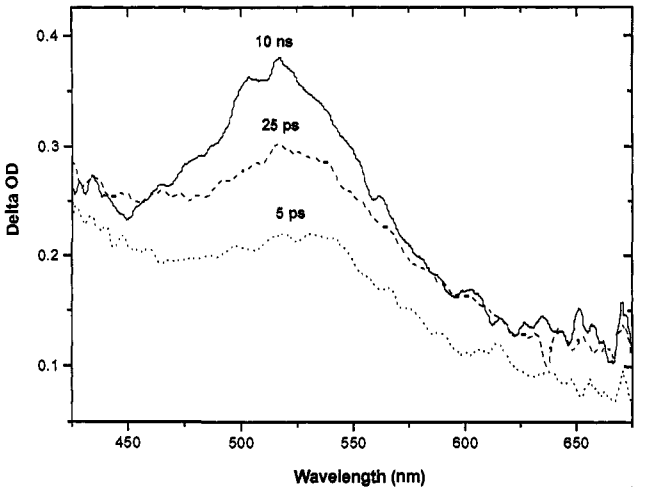

Figure 8. Transient absorbance spectra for AQC(2)/dGMP aqueous complexes recorded at 5 ps, 25 ps, and 10 ns delays after a 355 nm Nd-YAG laser pulse. [AQC(2)] = 2 mM, [dGMP] = 50 mM.

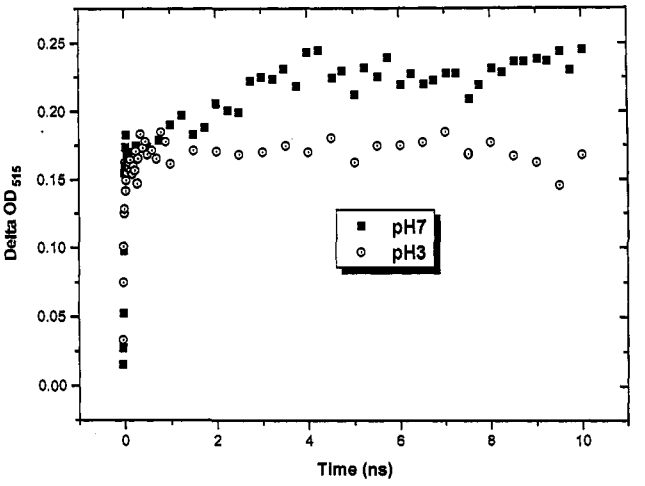

Figure 9. pH-dependent kinetics of $AQ^{\bullet-}$ formation (as monitored by the change in optical density at 515 nm) in aqueous AQC(2)/dGMP complexes. [AQC(2)] = 2 mM, [dGMP] = 50 mM.

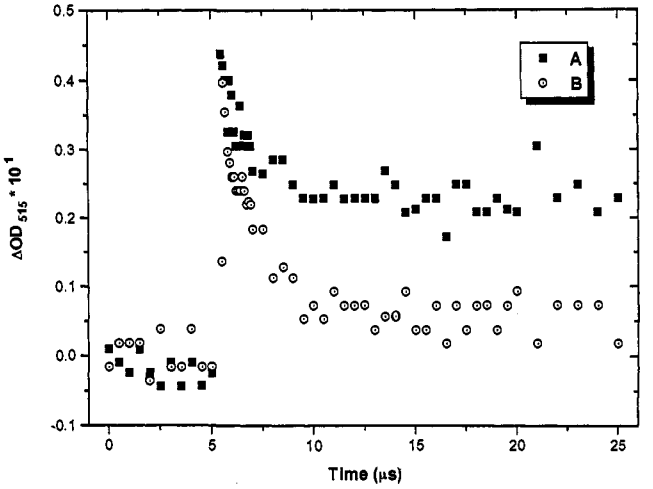

Figure 10. Decay of $AQ^{\bullet-}$ formed in AQC(2)/calf thymus DNA in (A) nitrogen-purged and (B) air-saturated samples. [AQC(2)] = 0.3 mM, [DNA] = 1.5 mM in PBS buffer.

540, 517, and 485 nm in acetonitrile, toluene, and ethanol, respectively.[32] Thus, slight differences in the binding environment for DNA-bound quinone radical anions could lead to significantly different values for the absorption maxima.

Additional experiments were performed on aqueous solutions of AQC(2) and a single DNA nucleotide, 2′-deoxyguanosine 5′-monophosphate (dGMP, Chart 1). Under the conditions used for the experiment (2.0 mM AQC(2), 50 mM dGMP), molecular complexes are formed between the quinone and the nucleotide as evidenced by a slight hypo- and bathochromicity apparent in the lowest energy quinone absorption band as well as by the appearance of a deep yellow color upon mixing of the two components. (An AQC(2) solution of this concentration is very faint yellow while a dGMP solution is colorless.) Neither the association constant nor the stoichiometry of the complex was determined due to the minor perturbation of the quinone absorption spectrum.

Excitation of the AQC(2)/dGMP complex as described above for the DNA-intercalation complexes also produces a transient absorption within the laser pulse but with λ_{max} = 515 nm (Figure 8). This transient is also assigned to the quinone radical anion ($AQ^{\bullet-}$); again, the different λ_{max} relative to water and DNA is attributed to the different environment within the quinone–nucleotide complex.[34] In contrast to the experiment with DNA, however, the transient species continues to grow out to 5 ns with no change in shape or λ_{max}. The growth of this band exhibits biphasic kinetics with the faster component being complete within 50 ps and the slower component extending out to 5 ns. Decreasing the pH of the solution from 7.0 to 3.0 has no effect on the fast component but eliminates the slow component (Figure 9). This observation strongly suggests that the secondary growth is due to a deprotonation reaction and that the pK_a of the precursor lies between 3.0 and 7.0.

The radical anion of AQC(2) produced in DNA decays over a period of ca. 10 μs under ambient, air-saturated conditions. In a nitrogen-purged sample, the decay of the quinone radical anion is retarded (Figure 10); complete reaction requires ca. 5 ms.

(B) Recycling of the Quinone. The oxygen-dependent decay of $AQ^{\bullet-}$ illustrated in Figure 9 suggests that AQ is regenerated simply by reduction of molecular oxygen:

$$AQ^{\bullet-} + O_2 \rightarrow AQ + O_2^{\bullet-} \qquad (1)$$

This reaction provides a pathway for recycling of the quinone photonuclease, which is required for the observed catalytic cleavage of DNA. The byproduct of this reaction, superoxide anion, can be readily detected by a two-step assay involving (*i*) its reduction of cytochrome *c* (cyt *c*) and (*ii*) inhibition of this reaction by the enzyme superoxide dismutase (SOD).[35] Thus, a solution containing DNA-intercalated AQC(2) and cyt *c* was irradiated at 350 nm. The visible absorption spectra clearly demonstrate reduction of cyt *c*, indicated by the growth with increasing irradiation time of the absorption band at 550 nm, characteristic of the reduced form ($Fe^{3+} \rightarrow Fe^{2+}$) of cyt *c* (Figure 11). In the presence of excess DNA relative to quinone, eq 1 suggests that AQC(2) should generate superoxide catalytically. Evidence for this proposal is presented in the inset to Figure 11, which demonstrates that AQC(2) sensitizes reduction of the cytochrome photocatalytically: at a level of five cytochromes per quinone, the observed >90% yield of reduced cyt *c* easily surpasses the stoichiometric limit (20%).

When SOD is also included in the reaction solution, the reduction of cyt *c* is inhibited (Figure 12). This establishes that cyt *c* is reduced by superoxide (eq 2) rather than by direct electron

$$\text{cyt } c(Fe^{3+}) + O_2^{\bullet-} \rightarrow \text{cyt } c(Fe^{2+}) + O_2 \qquad (2)$$

transfer from $AQ^{\bullet-}$ to the cytochrome. Figure 12 also demon-

(34) The oxidized guanine exhibits a tailing absorption in the same region as the quinone radical anion spectrum, but the extinction coefficient is expected to be 4–5 times lower than that of the reduced quinone (1000–2000 vs 6000–8000 M^{-1} cm^{-1}, ref 45).

(35) McCord, J. M.; Fridovich, I. *J. Biol. Chem.* **1969**, *244*, 6049–6055.

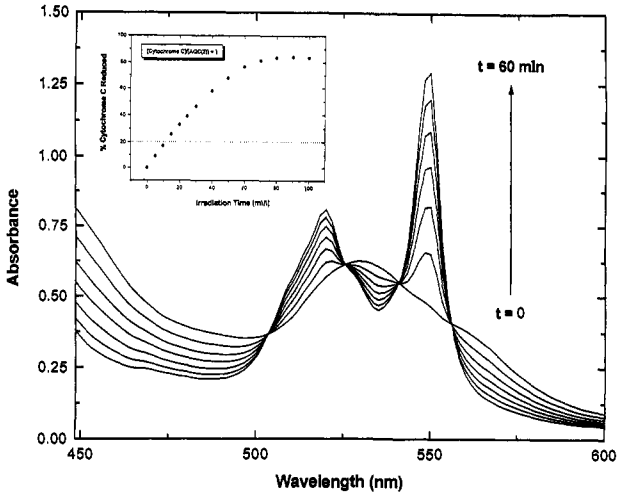

Figure 11. Visible absorbance spectra recorded at 10 min intervals during irradiation of AQC(2)/calf thymus DNA (10 μM quinone, 250 μM DNA in PE buffer) in the presence of 50 μM cytochrome *c*. Inset: yield of reduced cyt *c* as a function of irradiation time. The dashed line at 20% yield indicates the maximum yield attainable in the absence of turnover of the quinone.

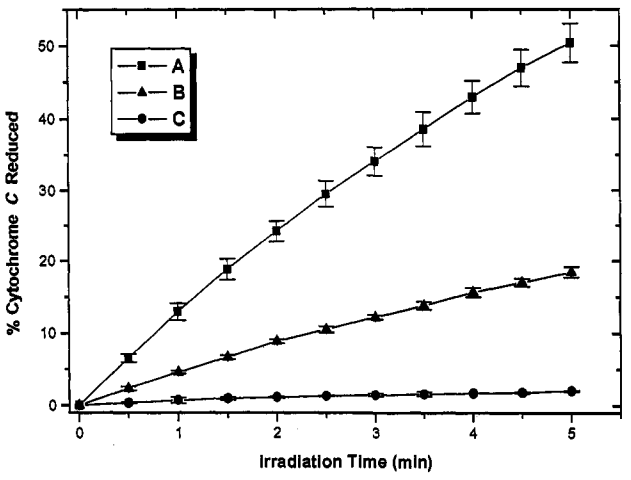

Figure 12. Plots of reduced cyt *c* yield as a function of irradiation time under various conditions. All samples contained 250 μM calf thymus DNA, 10 μM cyt *c*, 10 μg of catalase in 3 mL of PE buffer, and (A) 25 μM AQC(2), (B) 25 μM AQC(2) and 0.5 U/mL SOD, and (C) no quinone or SOD. The data points and error bars represent the means and standard deviations, respectively, of three separate measurements.

strates that the quinone must be present in order for photoreduction of cytochrome *c* to proceed.

It should be noted that inclusion of SOD has no effect on the decay of the quinone radical anion (data not shown), excluding the possibility that SOD inhibits reduction of the cytochrome by direct reaction with $Q^{\bullet-}$.

Photosensitized reductions of cytochrome *c* by DNA-bound AQC(2) and AQDS(2,6) were compared. As shown in Figure 13, AQC(2) promotes this reaction approximately three times more efficiently than does the disulfonamide analog. Assuming that the rate constant for eq 2 is independent of the source of the superoxide (i.e., AQC(2) vs AQDS(2,6)), then the data in Figure 13 indicate that generation of superoxide from irradiation of DNA-intercalated AQC(2) is 3-fold more efficient than from AQDS(2,6).

The detection of superoxide in the system raises the possibility that cleavage results not from the photo-oxidation of DNA by AQC(2) but rather by diffusible reduced oxygen species. Indeed, DNA cleavage has been reported in systems where superoxide was either added directly to the DNA (as KO_2[36]) or generated in situ.[3c] Superoxide can disproportionate to hydrogen peroxide

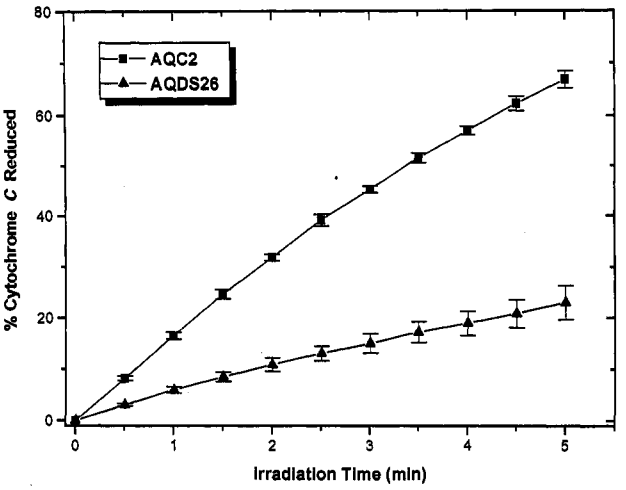

Figure 13. Comparison of cyt *c* reduction upon irradiation of calf thymus DNA-intercalated AQC(2) and AQDS(2,6). Samples contained 250 μM calf thymus DNA, 25 μM quinone, 10 μM cyt *c*, and 10 μg of catalase in 3 mL of PE. The data points and error bars represent the means and standard deviations, respectively, of three separate measurements.

and oxygen even in the absence of SOD (k_{dis} = 10^5 M^{-1} s^{-1}).[37] Reduction of the resulting peroxide via trace metal impurities can then lead to production of hydroxyl radicals (Fenton chemistry[38]), an established DNA cleavage agent.[39]

We studied the possible intermediacy of superoxide in the AQC(2)-sensitized cleavage of DNA using the simple fluorescence assay described earlier. Inclusion of SOD at a level that inhibits cyt *c* reduction by greater than 99% under the irradiation conditions results in less than 10% inhibition of cleavage. (The enzyme catalase was also added to scavenge the hydrogen peroxide produced by SOD.) Additionally, we have found that purging with N_2 prior to irradiation has no observable effect on photocleavage of supercoiled plasmid DNA by AQC(2).[40] Finally, SOD has been demonstrated to effectively inhibit DNA cleavage mediated by superoxide generated by a DNA-bound nuclease,[3c] in contrast to our observations. These results indicate that the superoxide produced by AQC(2) may be a minor contributor to the observed cleavage but that the dominant DNA-damaging chemistry results from the direct photo-oxidation of DNA by AQC(2).

Discussion

β-vs α-Substitution. Binding of the β-substituted AQ derivatives to DNA results in a significant hypochromicity, modest bathochromicity, and induction of circular dichroism in the lowest energy absorption band for the quinones. These results, taken together with other reported AQ intercalators, lead us to assign intercalation between adjacent base pairs as the DNA-binding mode for these quinones. In contrast, the α-substituted analogs AQC(1) and AQS(1) exhibit more modest hypochromicities and, for AQS(1), weaker and more complex induced CD bands which seem to indicate multiple binding modes. Furthermore, the α-substituted quinones fail to cleave DNA even after prolonged irradiation. Due to the weak and/or complex binding as well as the reduced reactivity of the α-substituted AQ derivatives, we

(36) Lesko, S. A.; Lorentzen, R. J.; Ts'o, P. O. P. *Biochemistry* **1980**, *19*, 3023–3028.
(37) McCord, J. M.; Crapo, J. D.; Fridovich, I. In *Superoxide and Superoxide Dismutases*; Michelson, A. M., McCord, J. M., Fridovich, I., Eds.; Academic Press: New York, 1977.
(38) Fenton, H. J. H. *J. Chem. Soc.* **1894**, *65*, 899–910.
(39) For reviews, see: (a) von Sonntag, C. In *Physical and Chemical Mechanisms in Molecular Radiation Biology*; Glass, W. A., Varma, M. N., Eds.; Plenum Press: New York, 1991. (b) von Sonntag, C. *The Chemical Basis of Radiation Biology*; Taylor & Francis: London, 1987.
(40) Koch, T.; Schuster, G. B. Unpublished data.

Scheme 1

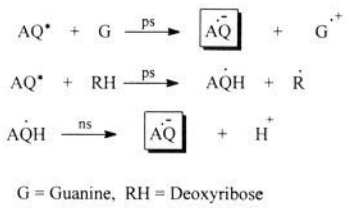

G = Guanine, RH = Deoxyribose

concentrated our efforts on development of the β-substituted compounds as DNA photonucleases.

Mechanistic Investigations: Formation of $AQ^{\bullet-}$ in the Reaction of AQ(2) with dGMP. The one-electron-reduced form of AQC(2), designated $AQ^{\bullet-}$, is the only product observed within 10 ns of excitation of aqueous quinone/dGMP complexes. The biphasic kinetics observed for the growth of $AQ^{\bullet-}$ in this system are attributed to reduction of the excited quinone by two distinct pathways (Scheme 1[41]): (*i*) electron transfer from the guanine component and (*ii*) hydrogen abstraction from the deoxyribose component. The second pathway yields the neutral semiquinone radical, $AQH^{\bullet-}$; subsequent deprotonation of this species then yields the radical anion. The fast appearance of $AQ^{\bullet-}$ is assigned to the electron transfer pathway while the slower growth reflects the hydrogen abstraction/deprotonation sequence. The effect of decreasing the pH from 7.0 to 3.0 supports this interpretation: at the lower pH, the fast component is unaffected but the slow component is eliminated. The pK_a for the anthrasemiquinone-2-sulfonate radical is 3.2;[31] we expect a similar value for $AQ^{\bullet-}$. The pH dependence of the latter step removes the possibility that the biphasic kinetics merely result from reaction of complexed versus free quinone molecules. On the basis of the change in absorbance at 515 nm after 10 ns for the two pH values, we estimate that 75% of the radical anion is formed by electron transfer while the remaining 25% results from H abstraction followed by deprotonation.

At pH = 3.0, $AQ^{\bullet-}$ formed by electron transfer from guanine is completely stable over the 10 ns time window of the experiment. Reaction with oxygen is insignificant while protonation does not occur on this time scale; however, back electron transfer could take place. The lack of back electron transfer in this system indicates that separation of the radical ion products occurs efficiently. This suggests that the quinone triplet state is responsible for generating the detected $AQ^{\bullet-}$: the resulting triplet radical ion pair would then exhibit slower charge recombination than the analogous singlet pair, thereby permitting separation to compete with back electron transfer. Anthraquinone is known to have a large intersystem crossing efficiency ($\Phi_{isc} = 0.9$),[42] consistent with this proposal.

Oxidation of DNA by AQ Photonucleases. The laser spectroscopic results for DNA-intercalated AQC(2) are considerably more complex than for the quinone/nucleotide system. A transient absorption appears within the laser pulse with λ_{max} = 555 nm. This species is neither the quinone triplet state nor the hydrogen-abstraction product, $AQH^{\bullet}$, both of which are expected to absorb below 400 nm with only a tailing absorption in the visible, based on literature spectra for anthraquinone-2-sulfonate in water.[31] Additionally, the observation of only the quinone radical anion in dGMP makes it highly improbable that the quinone singlet excited state would be observed in DNA and would live for approximately 200 ps. These observations suggest

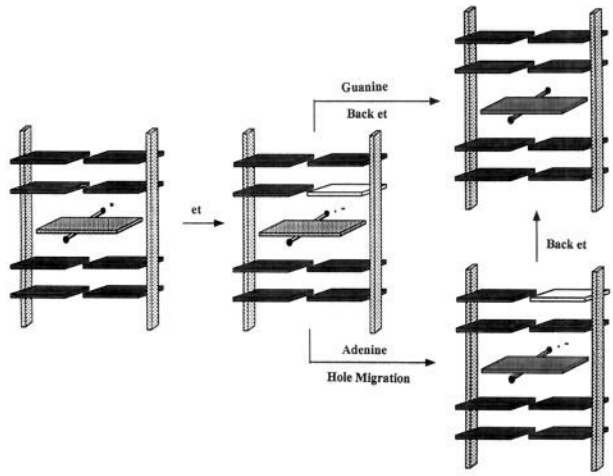

Figure 14. Schematic representation of electron transfer from an adjacent base (G or A) to an intercalated, photoexcited AQ. If the oxidized base (unshaded) is guanine, rapid back electron transfer occurs, while if it is adenine, the oxidation will migrate to a guanine site further along the DNA helix, retarding back electron transfer.

that the absorption band at 555 nm corresponds to $AQ^{\bullet-}$. This assignment requires a 55 nm red shift of this absorption when the quinone is intercalated into DNA rather than dissolved in water, a reasonable proposal in light of the strong solvent dependence of the anthraquinone radical anion, where λ_{max} = 540, 517, and 485 nm in acetonitrile, toluene, and ethanol, respectively.[32]

In CT DNA, $AQ^{\bullet-}$ is also produced within the laser pulse, but unlike the single nucleotide experiment, it immediately begins to decay with a concomitant shift in the absorption maximum to shorter wavelength. The decay process is attributed to back electron transfer, which proceeds because the electron donor (a DNA base) and acceptor (the intercalated quinone) remain in close proximity to one another after the forward reaction. Significantly, $AQ^{\bullet-}$ does not decay completely within 200 ps; a species absorbing at 545 nm remains. This absorption, too, is assigned to $AQ^{\bullet-}$. Thus the initial absorption at 555 nm is due to (at least) two distinct quinone radical anions exhibiting different absorption maxima and lifetimes. We attribute both of these products to electron transfer chemistry but occurring in different environments. Specifically, the position of the absorption maximum and the lifetime of $AQ^{\bullet-}$ are proposed to depend strongly on the adjacent DNA bases present at the intercalation site. Considering only one of the two adjacent base pairs for simplicity and assuming that the excited quinone will react with either adenine or guanine[43] (purines are more easily oxidized than pyrimidines[44]), two sets of electron transfer products can be envisioned: $AQ^{\bullet-}/A^{\bullet+}$ and $AQ^{\bullet-}/G^{\bullet+}$. Recent pulse radiolysis studies of dA-p-dG dinucleoside phosphates demonstrated that oxidation at adenine migrates quantitatively to guanine.[45] A similar process occurring in this system would cause a "hole" generated at adenine by electron transfer to the quinone to migrate to a guanine residue further along the helix (Figure 14). The back electron transfer would then be retarded, leading to a longer lifetime for $AQ^{\bullet-}$. This model then assigns the faster decaying, red-shifted component to the $AQ^{\bullet-}/G^{\bullet+}$ radical ion pairs, in which the hole remains on guanine and adjacent to the quinone radical anion.

(41) In Scheme 1 and throughout the discussion, the oxidized bases will be referred to as radical cations for simplicity. It should be noted, however, that deprotonation of the adenine and guanine radical cations should be quite fast, leaving neutral radicals. In solution, the proton is lost to the solvent, while in duplex DNA, it is likely shifted along the hydrogen bond coordinate toward the complementary base. Steenken, S. *Chem. Rev.* **1989**, *89*, 503–520.

(42) Wilkinson, F. *J. Phys. Chem.* **1962**, *66*, 2569–2574.

(43) Using a triplet energy of 2.73 eV (ref 41) and a reduction potential of –0.82 V (Prince, R. C.; Gunner, M. R.; Dutton, P. L. Reference 15, pp 29–32.) for anthraquinone and oxidation potentials of 0.71 and 0.81 V (ref 44) for guanine and adenine, respectively, we calculate driving forces of –1.20 and –1.10 eV for photoinduced electron transfer from G and A to the AQ photonucleases.

(44) Jovanovich, S. V.; Simic, M. G. *J. Phys. Chem.* **1986**, *90*, 974–979.

(45) Candeias, L. P.; Steenken, S. *J. Am. Chem. Soc.* **1993**, *115*, 2437–2440.

The longer timescale evolution of the spectrum involves primarily a further blue shift of the $AQ^{\bullet-}$ absorption band. The nanosecond time scale of these spectral changes is too slow for electron transfer reactions of the excited quinone as this species reacts within a few picoseconds. An alternative possibility is that $AQ^{\bullet-}$ dissociates from its intercalation site, resulting in the blue-shifted absorption. However, the dissociation kinetics experiments (Table 3) indicate that, for AQC(2), this process requires hundreds of microseconds. It seems unlikely that reduction of the quinone would accelerate its dissociation from DNA by some 4 orders of magnitude. Rather, we propose that these changes reflect the deprotonation of the semiquinone radical produced by photoinduced hydrogen atom abstraction from deoxyribose. The nanosecond dynamics of the shift are similar to the slower component of $AQ^{\bullet-}$ production in the reaction of AQC(2) with dGMP. (The expected growth in absorbance in the visible that should accompany the deprotonation is presumably countered by the ongoing back electron transfer between $AQ^{\bullet-}$ and $G^{\bullet+}$ separated by one or more base pairs.) Thus, the spectroscopy for both dGMP-complexed and DNA-intercalated AQC(2) exhibits fast production of $AQ^{\bullet-}$ by electron transfer and slower production by a hydrogen abstraction/deprotonation sequence. The distinction between the two systems and the resulting complexity for DNA-intercalated AQC(2) arise from (*i*) binding of the quinone in different environments within DNA and (*ii*) facilitated back electron transfer in DNA due to the inhibited separation of the radical ion products. Hole migration in DNA has the same effect, in part, as the physical separation of the radical ions in the dGMP system: stabilization of the electron transfer products.

The spectrum recorded at 20 ps for DNA-intercalated AQDS(2,6) is similar in magnitude to that of AQC(2) (Figure 6), indicating that the two quinones possess similar quantum yields for electron transfer with the DNA. The radical anions of the two species also decay to similar extents over the next 180 ps. However, the radical anion of AQDS(2,6) shows considerably more decay and less blue shift at 10 ns than observed for AQC(2), suggesting that the disulfonamide performs hydrogen atom abstraction less efficiently than does AQC(2). Thus the residual back electron transfer dominates the longer time scale dynamics for this quinone, resulting in a larger net decay of the absorbance.

Mechanism of DNA Cleavage by AQ Photonucleases. The competition between electron transfer and hydrogen atom abstraction raises questions about which of the two pathways actually leads to cleavage of the DNA backbone. In principle, cleavage could follow from either the oxidized base (electron transfer) or sugar (H abstraction). Although the vast majority of chemical nucleases initiate cleavage by the latter mechanism, oxidized bases produced by pulse radiolysis have been shown to lead to DNA strand breaks.[18]

Compelling evidence in favor of cleavage via hydrogen atom abstraction comes from comparison of the laser spectroscopic results for DNA-intercalated AQC(2) and AQDS(2,6). The spectra recorded at 20 ps for the two quinones indicate that, if anything, AQDS(2,6) undergoes electron transfer *more* efficiently than does AQC(2) (Figure 6). In both cases, the radical anion decays over the period of 200 ps to leave a residual, blue-shifted absorption. However, the radical anion of AQDS(2,6) exhibits considerably greater decay and less of a blue-shifted absorbance maximum on the nanosecond time scale. As described above, this observation is evidence that hydrogen atom abstraction is *less* efficient for AQDS(2,6) than for AQC(2). Significantly, we found that the DNA cleavage efficiency is approximately 5 times lower for AQDS(2,6) than for AQC(2). Thus, the spectroscopic data are consistent with cleavage resulting from H abstraction by the quinone photonuclease from deoxyribose.

Recycling of the Quinone. As shown in Figure 5, DNA cleavage by AQC(2) is photocatalytic. Therefore, the quinone radical anion must be converted back to its ground-state, fully oxidized form. The nanosecond laser spectroscopic results demonstrate that the lifetime of $AQ^{\bullet-}$ is significantly decreased by the presence of molecular oxygen (Figure 10). Meanwhile, irradiation of DNA-intercalated AQC(2) leads to the reduction of cytochrome *c* by a process which is inhibited by SOD, indicative of the presence of superoxide anion, $O_2^{\bullet-}$. Taken together, these results point toward oxidation of $AQ^{\bullet-}$ by molecular oxygen (eq 1). This process regenerates the quinone, forming the basis for the catalytic function of the anthraquinone photonucleases.

Scheme 2

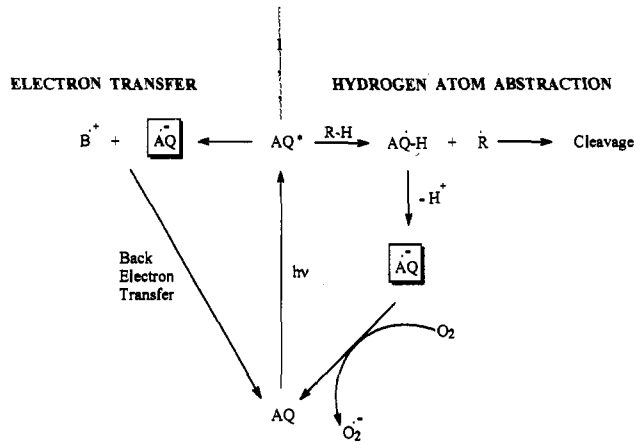

The lower efficiency of superoxide production by AQDS(2,6) is further evidence in support of a lower H-abstraction efficiency for this compound in comparison to AQC(2). The yield of superoxide should be independent of how the $AQ^{\bullet-}$ is formed, depending solely on how much of the radical anion is present. Since the two quinones appear to have similar quantum yields for electron transfer (on the basis of spectra at $t = 20$ ps, Figure 6), the significant difference in cytochrome *c* reduction (and, by inference, superoxide production) must be due to different H-abstraction efficiencies for the two quinones. Thus, the less efficient superoxide production by AQDS(2,6) is attributed to less efficient H abstraction. This is consistent with the time dependence of the various steps: even the slower component of the back electron transfer should be complete within a few tens of nanoseconds as indicated by the decay of $AQ^{\bullet-}$ for AQDS(2,6). However, the kinetic data shown in Figure 10 demonstrate that oxygen quenches $AQ^{\bullet-}$ 10–100 times slower than this. Therefore, superoxide will most likely result from reaction of molecular oxygen with $AQ^{\bullet-}$ formed by the H-abstraction pathway, giving rise to the different yields of reduced cytochrome *c* for AQC(2) and AQDS(2,6).

Scheme 2 summarizes the two oxidative pathways for reaction of the quinone photonucleases with DNA. Excitation of the intercalated quinone can lead either to electron transfer from an adjacent base (B) or to hydrogen atom abstraction from deoxyribose (RH). Products arising from the electron transfer chemistry regenerate starting materials primarily via back electron transfer. The hydrogen atom abstraction pathway produces (*i*) the sugar radical, which presumably decomposes to give cleavage of the DNA backbone, as well as (*ii*) the superoxide-producing $AQ^{\bullet-}$. Thus, the productive chemistry most likely arises by the H-abstraction pathway while the electron transfer pathway appears to constitute an energy-wasting cycle. The partitioning of the quinone between the two reaction modes will certainly have a profound effect on the DNA cleavage efficiency, as illustrated for AQC(2) and AQDS(2,6). It should be emphasized that the excited quinone must "choose" between these two reaction pathways within its excited-state lifetime (<20 ps). Thus, there is insufficient time for the quinone to reorient within the intercalation site, let alone dissociate from the DNA. As described below, the determining factor for distribution of excited quinone

molecules between the two oxidative pathways is most likely the orientation of the quinone within the intercalation site. Only those quinones which have at least one of their carbonyl oxygens sufficiently close to an abstractable deoxyribose hydrogen at the time of excitation will initiate cleavage; otherwise the quinone will be reduced by electron transfer.

Effect of Quinone Orientation on DNA Photocleavage. While the DNA-intercalation complexes formed by the AQ photonucleases have similar thermodynamic stabilities, the differences in induced CD spectra and cleavage efficiencies for the individual derivatives suggest that there are subtle, but functionally significant, differences in the structures of the complexes, specifically in the orientation of the intercalated quinone with respect to the adjacent base pairs. On the basis of the negative sign of the induced CD bands, the quinones appear to bind in an approximately parallel orientation, i.e. the long axis of the quinone skeleton is aligned parallel to the long axis of the adjacent DNA base pairs. However, the magnitude of the induced CD band exhibits significant variation within the series of compounds. Calculations point to three factors which influence the sign and intensity of an induced CD band for a DNA-intercalated chromophore: (*i*) local sequence, (*ii*) rotation, and (*iii*) translation of the chromophore within the binding site.[28,46]

Regarding the effect of the DNA sequence, for an approximately parallel orientation, binding at an AT step should result in an induced CD band that is approximately 4 times weaker than for binding at a GC step. The sequence preferences suggested by the binding constants for the synthetic polymers [poly(dA-dT)]$_2$ and [poly(dG-dC)]$_2$ (Table 2) indicate that the disulfonamide should have the weakest induced CD, contrary to the experimental results. However, the induced CD data can be rationalized by considering rotation as well as translation of the quinone within the binding pocket. Calculations indicate that rotation of an intercalated chromophore away from the parallel orientation will result in a weaker induced CD band. Alternatively, positioning of the chromophore toward either side of the intercalation site rather than directly in the center will also weaken the induced CD intensity. Either of these effects could account for the disparate cleavage efficiencies of the various AQ photonucleases, in light of the proposed cleavage mechanism. The laser spectroscopic data indicate that DNA cleavage is triggered by photoinduced hydrogen atom abstraction by one of the quinone oxygen atoms from a deoxyribose sugar in the DNA backbone. The results of Weisz and co-workers on the solid-state photoinduced intramolecular H abstraction by a series of enediones provide a striking example of the distance dependence of this type of reaction: an oxygen–hydrogen distance of 2.7 Å is sufficient to allow hydrogen abstraction while an analog in which the corresponding distance is 3.1 Å is completely unreactive.[47] Figure 15A depicts the relationship between the rotational orientation of the intercalated quinone and its ability to abstract a hydrogen from the DNA backbone.[48] A quinone which is completely parallel to the adjacent base pairs will have its oxygen atoms pointed away from the backbone. While this configuration is expected to produce the largest induced CD, it should also result in the lowest cleavage efficiency. Rotation of the quinone away from this parallel configuration will bring those oxygen atoms closer to the backbone, yielding progressively weaker induced CD bands but faster DNA cleavage.[49] An equally plausible model can be proposed for the cleavage efficiency being dependent on translational orientation of the bound quinone (Figure 15B). Displacement of the quinone toward the center of the intercalation site would lead to less efficient cleavage, since the quinone oxygen atoms would be at maximal distance from the deoxyribose hydrogens, but would yield the strongest induced CD band. Translation away from the center of the intercalation site decreases the critical O–H distance but weakens the induced CD band. In either case, the data of Weisz *et al.* indicate that an increase in this distance by as little as 0.4 Å is sufficient to abolish H abstraction. Circular dichroism spectroscopy clearly lacks the resolution required to distinguish between these two models. Future efforts will focus on the use of molecular modeling to gain insight into the structure of the AQ–DNA intercalation complexes.

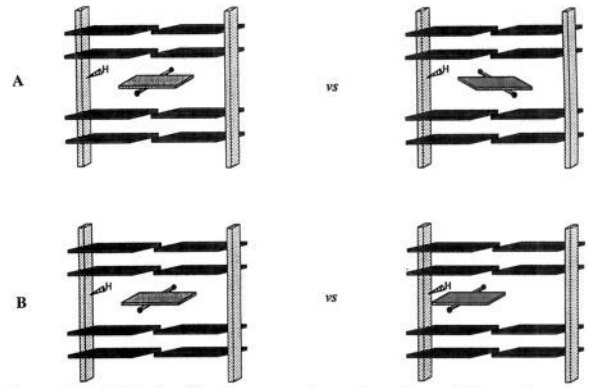

Figure 15. Relationship between the orientation of intercalated anthraquinone and the proximity to abstractable hydrogens on the DNA backbone. (A) Rotational model: The greatest π-stacking between the intercalator and the adjacent base pairs occurs in the orientation on the left, leading to the largest induced CD. This orientation also has the largest distance between the quinone oxygens (represented by the solid circles) and the DNA backbone, leading to the slowest rate of cleavage. (B) Translational model: Positioning of the quinone at the center of the intercalation site (depicted on the left-hand side of the figure) leads to the largest induced CD but also the greatest distance between the quinone oxygens and the DNA backbone, leading to the slowest rate of cleavage.

Quinone Recycling and Implications for Double-Stranded Cleavage. Recycling and turnover of AQC(2) is clearly demonstrated in Figure 5, establishing the β-substituted anthraquinones as catalytic photonucleases. As mentioned earlier, however, AQC(2) performs ds cleavage of DNA inefficiently. This is attributed to the failure of the quinone to remain bound at a given site for a sufficient period of time to permit attack of one strand, recycling, and then attack on the second strand. By assigning the decay observed in Figure 10 to direct oxidation of the quinone radical anion by molecular oxygen (eq 1), the chemical step needed for recycling is complete within 10 μs under ambient, air-saturated conditions. Meanwhile, the stopped-flow measurements reveal that this quinone is bound at a given DNA site, on average, for a few hundreds of microseconds. Unfortunately, with light intensities available from conventional lamps, it is improbable that a quinone at a single site will be excited twice before it dissociates from the DNA. Two strategies for improving the ds-cleavage efficiency of this class of reagents involve increasing either the light intensity or the residence time of the quinone (i.e., the time period over which it remains bound at a given site). The disubstituted analog AQDS(2,6) with its proposed threaded conformation is the first molecule we have synthesized on the basis of the latter strategy. The ds-cleavage efficiency of this synthetic photonuclease will be reported later.

(46) Lyng, R.; Rodger, A.; Nordén, B. *Biopolymers* **1991**, *31*, 1709–1720.
(47) Weisz, A.; Kaftory, M.; Vidavsky, I.; Mandelbaum, A. *J. Chem. Soc., Chem. Commun.* **1984**, 18–19.
(48) The intercalation complexes depicted in Figure 15 are, of course, simplifications. First of all, even though intercalation results in local unwinding of the duplex, there is still some twist to the DNA, unlike the perfectly parallel juxtaposition of the base pairs shown in the figure. Secondly, there are multiple hydrogen atoms available for abstraction on each strand. In fact, we cannot rule out the possibility that rotation and/or translation of the quinone within the intercalation site could lead to abstraction of different hydrogen atoms.
(49) Implicit in this discussion is the requirement that the quinone not reorient within the intercalation site during its excited-state lifetime. The observed lifetime of <20 ps for DNA-intercalated AQC(2) is consistent with this requirement.

Finally, the durability of these reagents is worth noting. In one experiment, a DNA/AQC(2) solution (10 base pairs per quinone) was irradiated until ca. 30% cleavage had occurred, based on the EB assay. This is a level of cleavage that greatly exceeds that required for any possible application of a synthetic nuclease. The amount of quinone was determined before and after its irradiation by absorption spectroscopy. Within the limits of detection, there was no decomposition of the quinone. Thus, prolonged and repeated use of these reagents, whether as small molecules or after tethering to DNA recognition elements, seems quite reasonable.

Conclusions

A series of amide and ammonium anthraquinone reagents were investigated as potential DNA cleavage agents. The molecules are functional only when substituted at the β-position. The quinones appear to be able to turnover indefinitely, making them robust photocatalysts. The photonuclease AQC(2) has been found to react with DNA by two competitive oxidative pathways: (1) electron transfer from an adjacent base and (2) hydrogen atom abstraction from a nearby deoxyribose unit. Cleavage evidently arises from the latter pathway since an analog (AQDS(2,6)) which appears to have a reduced H-abstraction efficiency also exhibits a lower cleavage efficiency. The electron transfer pathway seems to be an energy-wasting process, resulting primarily in back electron transfer. The orientation of the quinone within the intercalation site has a profound effect on the cleavage efficiency, consistent with the proposed hydrogen-abstraction pathway for initiation of cleavage. The reduced form of the quinone is converted back to its initial ground-state, fully oxidized form by back electron transfer as well as by reduction of molecular oxygen, yielding superoxide as a byproduct. These pathways regenerate the photonuclease and form the basis for its catalytic activity.

Experimental Section

General Procedures. Spectral data were recorded with the following spectrometers: GE QE-300 (300 MHz, ^{1}H; 75 MHz, ^{13}C), Cary 1E (UV–vis), SPEX 1681 FLUOROLOG (Fluorescence). Steady-state photolyses were carried out in a Rayonet photoreactor equipped with 350 nm lamps. Melting points were taken on a Büchi melting point apparatus and are uncorrected. Elemental analyses were performed by the University of Illinois Microanalysis Laboratory. High-resolution mass spectra were obtained from the University of Illinois Mass Spectroscopy Laboratory.

Materials. Ethidium bromide (EB) was purchased from Molecular Probes, Inc. (Eugene, OR) as a 10 mg/mL solution and diluted as necessary. 2′-Deoxyguanosine 5′-monophosphate (dGMP), horse heart cytochrome *c* (cyt *c*), superoxide dismutase from bovine erythrocytes (SOD), catalase from bovine liver, xanthine oxidase from buttermilk (XO), xanthine, calf thymus (CT) DNA, poly(deoxyadenylic-thymidylic acid) [poly(dA-dT)]$_2$, and poly(deoxyguanylic-deoxycytidylic acid) [poly(dG-dC)]$_2$ were purchased from Sigma (St. Louis, MO) and used as received. [Poly(dA-dT)]$_2$ and [poly(dG-dC)]$_2$ were suspended in PBS (10 mM phosphate, 100 mM NaCl, pH = 7.2) and stirred for 1 h. Concentrations were determined by the absorbance at 260 nm and the conversion factors supplied by the manufacturer: 0.1 mg/mL has A_{260} = 1.9 and 1.8 for [poly(dA-dT)]$_2$ and [poly(dG-dC)]$_2$, respectively. (One DNA base pair has molecular weight of approximately 660 g/mol.) Other concentrations were determined by UV–vis absorbance with the following extinction coefficients: ϵ_{480} = 5850 M^{-1} cm^{-1} for EB; ϵ_{252} = 13 700 M^{-1} cm^{-1} for dGMP; ϵ_{260} = 13 200 M^{-1} cm^{-1} for CT DNA (per base pair). Concentrations of DNA are given in terms of base pairs.

Enzymes were suspended in PE buffer (50 mM phosphate, 0.1 mM EDTA, pH =7.8). The catalase concentration was determined from its rate of decomposition of hydrogen peroxide.[50] XO activity was determined by the rate of reduction of cyt *c* upon addition of xanthine while SOD activity was determined by its inhibition of this process.[34] The cyt *c* concentration was determined by exhaustive reduction via xanthine/XO followed by measuring the absorbance at 550 nm (ϵ_{550} = 29 500 M^{-1} cm^{-1} for reduced cyt *c*).

All experiments involving CT DNA were performed in phosphate-buffered saline (PBS; 10 mM phosphate, 100 mM sodium chloride, pH = 7.2), unless otherwise noted. DNA solutions were prepared by dispersing the desired amount of DNA in buffer with stirring overnight. For experiments which required titration with DNA, the DNA solution was sonicated at 0 °C for 10 min using a Branson probe ultrasonicator. This significantly reduced the viscosity of the DNA solutions, permitting more accurate and precise titrations. Sodium dodecyl sulfate was recrystallized from 95% ethanol.

Anthraquinone-2-carbonyl Chloride. Anthraquinone-2-carboxylic acid (400 mg, 1.6 mmol) was suspended in 6 mL of thionyl chloride to give a cloudy brown mixture. Addition of 5 drops of dry DMF gave a clear brown solution which was then heated at reflux and stirred for 4 h. After removal of the solvent, the resulting brown solid was recrystallized from dichloromethane/ethyl acetate to afford 232 mg (0.86 mmol, 54% yield) of the desired acid chloride (mp 146–148 °C, lit. 147–148 °C[51]).

***N*-[4-[*N*-(*tert*-Butoxycarbonyl)amino]butyl]-2-anthraquinonecarboxamide [AQC(2)-boc].** A solution of 161 mg (0.86 mmol) of *N*-(*tert*-butoxycarbonyl)-1,4-diaminobutane, which was prepared from the reaction of 1,4-diaminobutane with di-*tert*-butyl dicarbonate,[51] in 5 mL of DMF and 1.5 mL of triethylamine was added to a solution of 232 mg (0.86 mmol) of anthraquinone-2-carbonyl chloride in 5 mL of DMF, giving a yellow solution which was initially cloudy but quickly cleared. The reaction solution was stirred at 55–60 °C for 20 h and then cooled to room temperature. The solution was poured into 25 mL of distilled water, yielding a precipitate. Filtration afforded 275 mg (0.65 mmol, 76% yield) of a light brown solid (mp 199–203 °C, lit. 201.5–202 °C[51]). The material was used without further purification.

***N*-(4-Aminobutyl)-2-anthraquinonecarboxamide Hydrochloride [AQC(2)].** The boc protecting group on the terminal amine was cleaved by dissolving 275 mg (0.65 mmol) of AQC(2)-boc in 4 mL of warm glacial acetic acid followed by addition of 8 mL of 1 M HCl in acetic acid. The yellow solution was stirred at 55–60 °C for 3 h and then poured into 35 mL of diethyl ether, giving a milky suspension. Filtration afforded 150 mg (0.42 mmol, 64% yield) of a light brown solid identified as AQC(2) on the basis of ^{1}H NMR, UV–vis, and mp data consistent with those of previously synthesized material.[51]

2,6-Anthraquinonedisulfonyl Chloride. Anthraquinone-2,6-disulfonic acid, disodium salt (7.8 g, 19 mmol) (Aldrich) was suspended in 100 mL of phosphoryl chloride, followed by addition of powdered phosphorus pentachloride (11.8 g, 57 mmol). The mixture was stirred at 95 °C for 16 h under a nitrogen atmosphere. After the removal of phosphoryl chloride by distillation, the residue was hydrolyzed by adding cold water while the solution cooled in an ice–water bath. The precipitate was filtered, washed twice with water, and dried in vacuo. Recrystallization from chlorobenzene gave 6.0 g (78%) of 2,6-anthraquinonedisulfonyl chloride (mp 248–249 °C, lit.[52] 250 °C).

***N*,*N*′-Bis[4-[*N*-(*tert*-butoxycarbonyl)amino]butyl]-2,6-anthraquinonedisulfonamide.** To a suspension of 0.41 g (1.01 mmol) of 2,6-anthraquinonedisulfonyl chloride in 120 mL of methylene chloride were added 3 mL of triethylamine and a solution of 0.5 g (2.22 mmol) of *N*-(*tert*-butoxycarbonyl)-1,4-diaminobutane in 10 mL of DMF (at this time, all substances were completely disolved). The reaction mixture was stirred at room temperature for 40 h and washed twice with water (400 mL), yielding a suspension. The suspension was diluted by adding 320 mL of ether and dried over sodium sulfate. After it was separated from sodium sulfate by decanting, the suspension was filtered with suction and the precipitate was washed once with ether to give 0.57 g (78%) of *N*,*N*′-bis[4-[*N*-(*tert*-butoxycarbonyl)amino]butyl]-2,6-anthraquinonedisulfonamide monohydrate (mp 213 °C (decomp)). The spectral data were as follows: ^{1}H NMR (300 MHz, DMSO-d_6) δ 1.29 (br s, 24 H), 2.75–2.79 (m, 8H), 3.34 (br s, 4H), 6.73 (t, J = 4.8 Hz, 2H, amide), 8.26 (d, J = 8.6 Hz, 2H aromatic), 8.41 (d, J = 8.6 Hz, 2H, aromatic), 8.52 (s, 2H, aromatic); ^{13}C NMR (75 MHz, DMSO-d_6) δ 26.82, 27.04, 28.64, 42.74, 77.77, 125.04, 128.77, 132.16, 134.30, 135.76, 146.23, 155.91, 155.95, 181.35. Anal. Calcd for $C_{32}H_{44}S_2N_4O_{10}\cdot H_2O$: C, 52.88; H, 6.38; N, 7.71. Found: C, 52.90; H, 6.33; N, 7.63.

***N*,*N*′-Bis(4-aminobutyl)-2,6-anthraquinonedisulfonamide Dihydrochloride [AQDS(2,6)].** To a hydrogen chloride saturated DMF solution (14 mL) was added 130 mg (0.18 mmol) of *N*,*N*′-bis[4-[*N*-(*tert*-butoxycarbonyl)amino]butyl]-2,6-anthraquinonedisulfonamide. The reaction mixture was stirred overnight. After the removal of DMF by distillation in vacuo, the residue was diluted by adding 2 mL of ethanol, 20 mL of

(50) Catalog, Sigma Chemical Co., 1994, p 222.

(51) Koch, T. Ph.D. Thesis, University of Copenhagen, Denmark, 1992.

(52) Fierz-David, H. E. *Helv. Chim. Acta* **1927**, *10*, 197–227.

methylene chloride, and 120 mL of ether. The precipitate was filtered, washed once with ether, and dried in vacuo overnight to give 82 mg (75%) of *N,N'*-bis(4-aminobutyl)-2,6-anthraquinonedisulfonamide dihydrochloride [AQDS(2,6)] monohydrate (mp > 240 °C (decomp)). The spectral data were as follows: ^{1}H NMR (300 MHz, DMSO-d_6) δ 1.40–1.55 (m, 6H, ammonium), 2.69 (br s, 3H, methylene), 2.75–2.80 (m, 3H, methylene), 3.34 (br s, 10H, methylene), 8.19 (t, J = 6.0 Hz, 2H, amide), 8.28 (dd, J = 8.4 Hz, 1.8 Hz, 2H, aromatic), 8.41 (d, J = 8.4 Hz, 2H, aromatic), 8.52 (d, J = 1.8 Hz, 2H, aromatic); ^{13}C NMR (75 MHz, DMSO-d_6) δ 24.52, 26.55, 38.58, 42.47, 125.04, 128.79, 132.23, 134.29, 135.78, 146.05, 181.29. Anal. Calcd for $C_{22}H_{30}S_2N_4O_6Cl_2 \cdot H_2O$: C, 44.07; 5.38; N, 9.35. Found: C, 44.17; H, 5.30; N, 9.45.

2-Anthraquinonesulfonyl Chloride. Anthraquinone-2-sulfonic acid, sodium salt (15.0 g, 46 mmol) (Aldrich) was suspended in phosphoryl chloride (100 mL) (Aldrich), followed by adding powdered phosphorus pentachloride (10.0 g, 48 mmol). The mixture was stirred at 90 °C for 3.5 h under nitrogen atmosphere. After the removal of phosphoryl chloride by distillation, the residue was hydrolyzed by adding cold water while the mixture was cooled in an ice–water bath. The precipitate was filtered, washed twice with water, and dried in vacuo. Recrystallization from methylene chloride and ether gave 11.1 g (79%) of 2-anthraquinonesulfonyl chloride (mp 194–195 °C, lit. 210 °C,[52] 193 °C,[53] 197 °C[54]).

***N*-[4-[*N*-(*tert*-Butoxycarbonyl)amino]butyl]-2-anthraquinonesulfonamide.** To 40 mL of DMF were added 0.63 g (2.05 mmol) of 2-anthraquinonesulfonyl chloride, 1.1 mL of triethylamine, and 0.50 g (2.22 mmol) of *N*-(*tert*-butoxycarbonyl)-1,4-diaminobutane. The mixture was stirred for 3 h and diluted by adding 300 mL of water. The precipitate (at the top) was filtered with suction, washed twice with water, and recrystallized from 95% ethanol to give 0.45 g (48%) of *N*-[4-[*N*-(*tert*-butoxycarbonyl)amino]butyl]-2-anthraquinonesulfonamide (mp 150–151 °C). The spectral data were as follows: ^{1}H NMR (300 MHz, $CDCl_3$) δ 1.40 (s, 9H, methyl), 1.46–1.58 (m, 4H, methylene), 3.01–3.09 (m, 4H, methylene), 4.62 (br s, 1H, amide), 5.46 (br s, 1H, amide), 7.82–7.87 (m, 2H, aromatic), 8.24–8.35 (m, 3H, aromatic), 8.44 (d, J = 9.9 Hz, 1H, aromatic), 8.73 (d, J = 1.5 Hz, 1H, aromatic); ^{13}C NMR (75 MHz, DMSO-d_6) δ 26.84, 27.04, 28.65, 42.71, 77.75, 124.97, 127.37, 128.60, 131.99, 133.45, 134.23, 135.24, 135.71, 145.97, 156.20, 182.06, 182.13. Anal. Calcd for $C_{23}H_{26}N_2SO_6$: C, 60.25; H, 5.72; N, 6.11. Found: C, 60.18; H, 5.74; N, 6.08.

***N*-(4-Aminobutyl)-2-anthraquinonesulfonamide Hydrochloride [AQS(2)].** To 20 mL of slightly warm methanol were added 210 mg (0.46 mmol) of *N*-[4-[*N*-(*tert*-butoxycarbonyl)amino]butyl]-2-anthraquinonesulfonamide and 20 mL of 1 N HCl ether solution. The reaction mixture was stirred under nitrogen for 2.5 h and diluted by adding 100 mL of ether. The precipitate was filtered with suction, washed once with ether, and dried in vacuo for 48 h to give 159 mg (87%) of *N*-(4-aminobutyl)-2-anthraquinonesulfonamide hydrochloride [AQS(2)] (mp > 230 °C (decomp)). The spectral data were as follows: ^{1}H NMR (300 MHz, DMSO-d_6) δ 1.42–1.49 (m, 3H, ammonium), 2.69 (br s, 2H, methylene), 2.78 (t, J = 6.3 Hz, 2H, methylene), 3.33 (br s, 4H, methylene), 7.82–7.97 (m, 3H, aromatic and amide), 8.21–8.27 (m, 3H, aromatic), 8.38 (d, J = 8.1 Hz, 1H, aromatic), 8.51 (s, 1H, aromatic); ^{13}C NMR (75 MHz, DMSO-d_6) δ 24.53, 26.55, 38.53, 42.40, 124.96, 127.34, 128.63, 132.06, 133.42, 134.16, 135.28, 135.68, 145.80, 145.88, 182.03, 182.09; HRMS (FAB) m/z 359.1067 (359.1066 calcd for $C_{18}H_{19}N_2SO_4$). Anal. Calcd for $C_{18}H_{19}N_2SO_4Cl$: C, 54.75; H, 4.85; N, 7.09; Cl, 8.98. Found: C, 54.71; H, 4.83; N, 7.08; Cl, 8.94.

1-Anthraquinonesulfonyl Chloride. 1-Anthraquinonesulfonyl chloride (mp 215–216 °C, lit. 210–211 °C,[55] 216–218 °C[56]) was prepared in 72% yield from 9.0 g (29 mmol) of 1-anthraquinonesulfonic acid, sodium salt (Eastman) and 10 g (48 mmol) of phosphorus pentachloride in 100 mL of phosphoryl chloride by following the procedure described above for the synthesis of 2-anthraquinonesulfonyl chloride.

***N*-[4-[*N*-(*tert*-Butoxycarbonyl)amino]butyl]-1-anthraquinonesulfonamide.** To 50 mL of DMF were added 0.63 g (2.05 mmol) of 1-anthraquinonesulfonyl chloride, 1.5 mL of triethylamine, and 0.5 g (2.22 mmol) of *N*-(*tert*-butoxycarbonyl)-1,4-diaminobutane. The reaction mixture was stirred for 2 h and poured into 200 mL of water, giving a milk-like solution. After stirring for 1 h and standing at room temperature overnight, a precipitate was formed on top of the solution. The precipitate was filtered, washed once with water, then dissolved in 100 mL of methylene chloride, and dried over sodium sulfate. After the methylene chloride solution was concentrated to about 5 mL, the residue was diluted by adding 250 mL of ether; a light yellow precipitate was formed and collected by filtration to give 0.79 g (84%) of *N*-[4-[*N*-(*tert*-butoxycarbonyl)amino]butyl]-1-anthraquinonesulfonamide (mp 114–115 °C). The spectral data were as follows: ^{1}H NMR (300 MHz, $CDCl_3$) δ 1.37 (br s, 9H, methyl), 1.44–1.57 (m, 4H, methylene), 3.01–3.13 (m, 4H, methylene), 4.50–4.52 (m, 1H, amide), 6.75 (t, J = 6.0 Hz, amide), 7.81–7.85 (m, 2H, aromatic), 7.93 (t, J = 7.8 Hz, 1H, aromatic), 8.24–8.27 (m, 2H, aromatic), 8.59 (t, J = 7.8 Hz, 2H, aromatic); ^{13}C NMR (75 MHz, $CDCl_3$) δ 27.10, 27.20, 28.33, 39.92, 43.32, 79.22, 127.05, 127.95, 131.80, 132.01, 132.06, 133.84, 134.23, 134.68, 134.81, 135.88, 136.09, 140.85, 155.87, 181.74, 184.23. Anal. Calcd for $C_{23}H_{26}SN_2O_6$: C, 60.25; H, 5.72; N, 6.11. Found: C, 60.23; H, 5.71; N, 6.10.

***N*-(5-Aminobutyl)-1-anthraquinonesulfonamide Hydrochloride [AQS(1)].** AQS(1) (mp 185 °C (decomp)) was prepared in 74% yield from 0.22 g (0.47 mmol) of *N*-[4-[*N*-(*tert*-butoxycarbonyl)amino]butyl]-1-anthraquinonesulfonamide and 15 mL of 1 N HCl ether solution in 10 mL of methanol by following the procedure described above for the synthesis of AQS(2). The spectral data were as follows: ^{1}H NMR (300 MHz, DMSO-d_6) δ 1.48 (br s, 3H, ammonium), 2.66 (t, J = 6.6 Hz, 2H, methylene), 2.90–2.94 (m, 2H, methylene), 3.33 (br s, 4H, methylene), 7.90–7.98 (m, 3H, aromatic and amide), 8.07 (t, J = 7.8 Hz, 1H, aromatic), 8.14–8.16 (m, 2H, aromatic), 8.44 (d, J = 13.5 Hz, 1H, aromatic), 8.47 (d, J = 13.5 Hz, 1H, aromatic); ^{13}C NMR (75 MHz, DMSO-d_6) δ 24.46, 26.76, 38.55, 42.91, 126.97, 127.45, 131.47, 132.03, 132.38, 134.35, 134.71, 135.12, 135.38, 135.61, 136.71, 141.02, 182.03, 182.07. Anal. Calcd for $C_{18}H_{19}SN_2O_4Cl$: C, 54.75; H, 4.85; N, 7.09. Found: C, 54.37; H, 5.12; N, 6.80.

***N*-[4-[*N*-(*tert*-Butoxycarbonyl)amino]butyl]-1-anthraquinonecarboxyamide.** This compound (mp 168–169 °C) was prepared in 98% yield from 0.32 g (1.18 mmol) of 1-anthraquinonecarbonyl chloride, 0.28 g (1.25 mmol) of *N*-(*tert*-butoxycarbonyl)-1,4-diaminobutane, and 1.5 mL of triethylamine in 100 mL of methylene chloride and 2 mL of DMF, following the procedure described above for the synthesis of *N,N'*-bis[4-[*N*-(*tert*-butoxycarbonyl)amino]butyl]-2,6-anthraquinonedisulfonamide. The spectral data were as follows: ^{1}H NMR (300 MHz, $CDCl_3$) δ 1.40 (s, 9H, methyl), 1.64–1.71 (m, 2H, methylene), 1.74–1.81 (m, 2H, methylene), 3.19–3.23 (m, 2H, methylene), 3.58 (q, J = 6.3 Hz, 2H, methylene), 4.85 (br s, 1H, amide), 6.14 (br s, 1H, amide), 7.65–7.80 (m, 4H, aromatic), 8.22–8.34 (m, 3H, aromatic); ^{13}C NMR (75 MHz, DMSO-d_6) δ 26.52, 27.51, 28.73, 39.15, 77.82, 127.05, 127.33, 127.66, 132.80, 133.77, 133.97, 134.27, 134.39, 134.87, 135.20, 139.72, 156.06, 168.99, 182.39, 182.71; HRMS (FAB) m/z 423.1921 (423.1920 calcd for $C_{24}H_{26}N_2O_5 + H^+$). Anal. Calcd for $C_{24}H_{26}N_2O_5 \cdot {}^1/_2H_2O$: C, 66.81; H, 6.31; N, 6.49. Found: C, 66.53; H, 6.53; N, 6.73.

***N*-(4-Aminobutyl)-1-anthraquinonecarboxyamide Hydrochloride [AQC(1)].** A solution of 0.16 g (0.38 mmol) of *N*-[4-[*N*-(*tert*-butoxycarbonyl)amino]butyl]-1-anthraquinonecarboxyamide in 100 mL of HCl saturated ethyl acetate was stirred overnight. The solution was concentrated to about 20 mL and diluted by adding 100 mL of ether. The resulting precipitate was filtered and washed once with ether to give 0.13 g (95%) of AQC(1) (mp 237 °C (decomp)). The spectral data were as follows: ^{1}H NMR (300 MHz, DMSO-d_6) δ 1.59–1.65 (m, 3H, ammonium), 2.82 (br s, 2H, methylene), 3.26 (t, J = 6.3 Hz, 2H, methylene), 3.64 (br s, 2H, methylene), 7.70–7.72 (m, 1H, aromatic), 7.88–8.26 (m, 7H, aromatic and amide); ^{13}C (75 MHz, DMSO-d_6) δ 24.94, 26.15, 38.68, 38.83, 127.05, 127.38, 127.73, 130.50, 132.50, 132.80, 133.29, 133.90, 134.31, 134.46, 134.90, 135.26, 139.56, 169.06, 182.39, 182.70; HRMS (FAB) m/z 323.1393 (323.1396 calcd for $C_{19}H_{19}N_2O_3$). Anal. Calcd for $C_{19}H_{19}N_2O_3Cl \cdot {}^1/_2H_2O$: C, 62.04; H, 5.48; N, 7.62. Found: C, 61.67; H, 5.43; N, 7.82.

Determination of Binding Constants. UV–vis method: A buffered solution of the appropriate AQ derivative (typically 40 μM quinone in a 1.0 cm cuvette) was titrated with a concentrated DNA solution. The optical density of the solution at 333 nm was measured initially and after each addition on a Cary 1E spectrophotometer (Varian Techtron Pty. Ltd., Victoria, Australia). (DNA was also added to the reference cuvette to minimize scattering contributions to the absorbance.) The change in optical density together with the extinction coefficients for the quinone in buffer and DNA was used to calculate α, the fraction of bound quinone.[20b] Scatchard analysis for the data $0.20 \leq \alpha \leq 0.80$ then yielded the equilibrium binding constant. Each sample was done in triplicate.

Fluorescence method: The equilibrium binding constants of ethidium bromide (EB) with calf thymus DNA, $[poly(dG\text{-}dC)]_2$, and $[poly(dA\text{-}dT)]_2$ were measured by a fluorescence titration method in the absence

(53) King, J. F.; Smith, D. J. H. *Can. J. Chem.* **1965**, *43*, 1870–1874.
(54) MacHoul, D. A. *Chem. Ber.* **1880**, *13*, 692–694.
(55) Meyer, H.; Schlegl, K. *Monatsh. Chem.* **1913**, *34*, 561–577.
(56) *The Dictionary of Organic Compounds*; Chapman and Hall: New York, 1982; p 388.

and presence of AQC(2), AQS(2), and AQDS(2,6). Samples typically consisted of 2.5 μM DNA in 2.5–3.0 mL of PBS and were titrated with 10 μL aliquots of 50–60 μM EB. Additions of 10 μL aliquots of a solution containing 5.0 μM DNA and the appropriate concentration of quinone were made at the same time in order to maintain the concentration of DNA as well as the ratio of quinone to DNA.[57] Spectra were obtained with excitation at 510 nm and emission from 550–650 nm. The integrated spectra were used for the data analysis. The data were corrected for absorbance by the ethidium and then analyzed according to the method of LePecq and Paoletti to obtain the bound (c_b) and free (c_f) concentrations of EB.[21] Plotting r/c_f vs r (where $r = c_b/[\text{DNA}]$) and fitting to the McGhee–von Hippel equation[58] yielded a binding constant (K_{EB}) for EB. In the absence of quinone, this value is equal to the intrinsic equilibrium binding constant for EB. In the presence of quinone, K is an apparent binding constant and can be used to calculate the equilibrium binding constant for the quinone (K_{AQ}) using the following equation:

$$K = K_{EB}/[1 + K_{AQ}{}^{*}C_f^{AQ}]$$

where C_f^{AQ} is approximately equal to the total concentration of quinone. The procedure was done at two separate quinone concentrations, usually between 2.0 and 20 μM depending on how effectively the quinone competed with EB for binding sites.[59]

Induced Circular Dichroism (CD) Spectroscopy. CD spectra were recorded on a JASCO J-270 instrument. Six accumulations were collected for each sample. Solutions were prepared containing 0.2 mM quinone in PBS. Spectra were recorded from 500 to 300 nm in the presence of 0, 0.4, 0.8, and 1.6 mM sonicated CT DNA.

Stopped-Flow Spectrophotometry. The procedure is outlined for AQDS(2,6): Solutions containing (A) DNA/AQDS(2,6) (10 DNA base pairs per quinone, 0.1 mM quinone) in PBS and (B) 50 mM SDS in buffer (10 mM phosphate, 50 mM NaCl, pH = 7.2) were loaded into the separate sample holders of a Union Giken (Osaka, Japan) RA-401 stopped-flow spectrophotometer. The two solutions were mixed rapidly (ca. 1 ms) within a 2 mm quartz cell using pressurized nitrogen gas. Dissociation of the quinone from the DNA was monitored as a time-dependent increase in optical density at 330 nm. The growth was fit to a single exponential; duplicate trials gave a dissociation rate constant (k_d) of 360 ± 60 s^{-1}. Dissociation was too rapid to be fit reliably for AQC(2) and AQS(2), overlapping with the instrumental mixing time.

Ethidium Bromide Assay for DNA Cleavage. Cleave of DNA reduces the number of available binding sites for the intercalator ethidium bromide (EB), resulting in a diminished fluorescence intensity for an EB-containing DNA solution.[30] After preparation of a DNA/quinone solution (260 μM DNA bp, 26 μM quinone), 100 μL was removed and added to 2.4 mL of PBS. Then, 40 μL of a 1.28 mM EB stock solution was added. The integrated fluorescence spectrum was then measured from 525 to 800 nm with excitation at 510 nm. The remaining DNA/quinone solution was irradiated in a Rayonet photoreactor (nine 350 nm tubes), with aliquots removed at various times and analyzed as described above.

The percentage of binding sites remaining at a given time (t) was calculated from the following equation:

$$\%\ \text{binding sites remaining} = 100 \times \left(1 - \frac{I_0 - I_t}{I_0 - I_{PBS}}\right)$$

where I_0, I_t, and I_{PBS} correspond to the integrated fluorescence intensities before irradiation, after t min of irradiation, and in DNA-free buffer, respectively. I_{PBS} is taken as 0% binding sites remaining.[60]

Photostability of AQC(2). A sample was prepared containing 0.08 mM AQC(2) and 0.8 mM calf thymus DNA in PBS. A 1.0 mL sample of the solution was added to 2.0 mL of 25 mM sodium dodecyl sulfate (SDS) in PBS.[61] The absorbance of this solution at 333 nm was then measured. Another aliquot of the DNA/AQC(2) solution was removed for analysis by the ethidium bromide binding assay. The remaining sample was then irradiated in a Rayonet photoreactor for 7 min (seven lamps, λ = 350 nm). After irradiation, aliquots were removed for UV analysis and the ethidium bromide binding assay as described above.

A second sample was prepared consisting of 0.08 mM AQC(2) in PBS. The absorbance of this solution at 333 nm was measured before and after irradiation as described for the DNA-containing sample. Dilution into SDS was not required in the absence of DNA.

Laser Spectroscopy of DNA/Quinone Complexes. Samples for picosecond laser spectroscopy contained 1.5 mM quinone and 7.5 mM sonicated CT DNA in PBS. Samples were excited at 355 nm with a 20 ps Nd-YAG laser pulse, and transient absorbance spectra were recorded at delays of –50, 20, and 200 ps as well as 10 ns using instrumentation described elsewhere.[62] Decay of the transient observed at 20 ps was estimated on the basis of the peak intensities at the two later delays. Longer time scale decay of this transient for AQC(2)/DNA was investigated using a 20 ns pulse at 308 nm from a XeCl excimer laser. The sample (0.3 mM AQC(2), 1.5 mM CT DNA in PBS, 1 cm quartz cell) was either air-equilibrated or purged with nitrogen for 15 min prior to the experiment. Decay of the transient was monitored at 520 nm.

Laser Spectroscopy of AQC(2)/dGMP Complexes. A solution of AQC(2) (2 mM) and dGMP (50 mM) in water was excited at 355 nm as described above. Transient absorbance spectra were acquired at 50 different delays ranging from –50 ps to 10 ns. The experiment was performed at pH = 7.0 and 3.0, the desired pH being obtained by addition of HCl and checked by a pH meter. The change in absorbance at 515 nm was plotted versus time for the two samples, with the pH = 3.0 data normalized to that at 7.0 by multiplying by the ratio of the changes in absorbance at a 100 ps delay. This normalization accounts for differences in laser power for the two experiments and is justified by the observation that the kinetics of the initial growth are pH-independent.

Photosensitized Reduction of Cyt *c* by DNA-Bound AQC(2). A sample was prepared containing 250 μM CT DNA, 10 μM AQC(2), 50 μM cyt c, and 10 μg of catalase in PE buffer. UV–vis absorbance spectra were recorded before and after various irradiation times (Rayonet, eight lamps). The percentage of reduced cyt c at a given time (t) was calculated using the following formula:

$$\%\ \text{cyt } c_{red} = 100 \times \left[\frac{A(550)_t - A(550)_0}{A(550)_0 \times \left(\frac{\epsilon(550)_{red}}{\epsilon(550)_{ox}} - A(550)_0\right)}\right]$$

where $A(550)_0$ and $A(550)_t$ are the absorbances at 550 nm initially and after t min of irradiation, respectively. $\epsilon(550)_{red}$ = 29 500 M^{-1} cm^{-1} and $\epsilon(550)_{ox}$ = 8900 M^{-1} cm^{-1} are the extinction coefficients of the reduced and oxidized forms of cyt c.

In other experiments, 3.0 mL samples were prepared containing 250 μM CT DNA, 25 μM AQC(2), 10 μM cyt c, and 10 μg of catalase in PE buffer. The samples were irradiated at 350 nm (Rayonet, four lamps) with the absorbance at 550 nm recorded every 30 s up to 5 min. The experiment was repeated (a) in the presence of 1.5 U of SOD, (b) in the absence of quinone, and (c) with AQDS(2,6) replacing AQC(2). Each experiment was done in triplicate with the percent cyt c reduction calculated as described above.

Effect of SOD on DNA Cleavage by AQC(2). Samples were prepared containing 250 μM CT DNA in PBS (2.0 mL total volume). The samples were irradiated at 350 nm (Rayonet, four lamps) in the absence or presence of 10 U of SOD and 10 μg of catalase. For those samples lacking the enzymes, PE buffer was added in a volume equal to that present in the enzyme-containing samples. This is important since DNA cleavage by AQC(2) is inhibited by EDTA in a concentration-dependent manner. Each sample was done in triplicate with the extent of cleavage after 10 min of irradiation being measured by reduced binding of EB to the DNA in the fluorescence assay described above.

Acknowledgment. We thank Professor L. Hager of the Biochemistry Department of the University of Illinois and Dr. B. Bertanogilli of the Plant Pathology Department for assistance with the stopped-flow experiments. This work was supported by a grant from the National Institutes of Health, for which we are grateful.

(57) Reinhardt, C. G.; Krugh, T. R. *Biochemistry* **1978**, *17*, 4845–4854.
(58) Equation 10 from the following: McGhee, J. D.; von Hippel, P. H. *J. Mol. Biol.* **1974**, *86*, 469–489.
(59) Sari, M. A.; Battioni, J. P.; Dupré, D.; Mansuy, D.; Le Pecq, J. B. *Biochemistry* **1990**, *29*, 4205–4215.
(60) It should be noted that it is unlikely that the DNA is completely digested, leaving only free bases and damaged sugar phosphates. The remaining DNA probably contains some single-stranded (ss) DNA. Binding of EB to ss DNA can also lead to an enhancement in fluorescence, but not as large as for ds DNA.[20] Therefore, if ss DNA remains in the sample, I_t will never reach I_{PBS} and eq 1 underestimates the actual cleavage.
(61) Trapping the quinone within SDS micelles removes the hypochromicity of the absorbance band, which depends on the amount of DNA-bound quinone.